AN EXPERIMENTAL SINGLE FOURIER TRANSFORM OPTICAL PROCESSOR APPLIED TO FILM GRAIN ANALYSIS AND A SHIP WAVE DETECTION METHOD

by

Robert Dale Ferguson

United States Naval Postgraduate School

THESIS

AN EXPERIMENTAL SINGLE FOURIER TRANSFORM OPTICAL PROCESSOR APPLIED TO FILM GRAIN ANALYSIS AND A SHIP WAVE DETECTION METHOD

by

Robert Dale Ferguson

December 1969

An Experimental Single Fourier Transform Optical Processor Applied to Film Grain Analysis and A Ship Wave Detection Method

by

Robert Dale Ferguson
Lieutenant, United States Navy
B. S., University of Washington, 1963

Submitted in partial fulfillment of the
requirements for the degrees of

ELECTRICAL ENGINEER

and

MASTER OF SCIENCE IN ELECTRICAL ENGINEERING

From the

NAVAL POSTGRADUATE SCHOOL
December 1969

ABSTRACT

A single Fourier transform optical system was constructed and tested on two projects. First, film grain in a single Fourier transform operation was studied and a mathematical model of the film grain and a semi-quantitative prediction of the grain's transform were developed and verified using the experimental system. The film grain was found to have a noise-like spatial frequency spectrum which was a decreasing function of frequency, and that this spectrum could be considered Gaussian only in the case of fine grain films containing binary signal images. Second, the system was used to investigate a proposed method of detecting a ship wave. A deterministic relation between a ship wave and the Fourier transform of its photograph was shown to exist. A sample photograph of a ship wave was inserted into the system and operated on by a matched filter rotated in a plane normal to the optical axis. The output light intensity was determined as a function of the filter angular position. The output intensity when considered to be periodic was found to have a discernible spectral content due to the ship wave.

TABLE OF CONTENTS

LIST OF TABLES

LIST OF ILLUSTRATIONS

TABLE OF SYMBOLS

a_T	radius of aperture of class a.
C	constant.
d	total optical path length.
d_1	separation of P1 and P2.
D	photographic density.
D_{min}	minimum, or no-exposure, photographic density.
D_{max}	maximum, or saturated, photographic density.
E	photographic exposure.
$f(x_1, y_1)$	light transmitted at P1.
$f_a(x_2, y_2)$	Fourier transform of the set of apertures called class a.
$f(x_2, y_2)_a$	Fourier transform of a single aperture of class a.
f_i	source light.
$f_T(x_2, y_2)$	total Fourier transform of apertures of all classes.
f_o	source light magnitude.
f_1	light trasmitted by P1.
f_2	light incident of P2.
f_{2a}	Fourier transform due to circular aperture model.
f_{2s}	Fourier transform due to circular stop model.
F	focal length.
$\mathcal{F}$	Fourier transform operation.
g	acceleration due to gravity.
H(x, y)	wave height structure on the sea surface.

I_p	light intensity.
J_1	first-order Bessel function.
k	radian wave number.
K	constant.
ℓ	normalized light intensity.
L	principal plane of simple lens.
m	magnification.
M	camera illumination.
N	luminance of the sky in the direction reflected into the camera.
N_a	total number of apertures in class a.
P1	input plane.
P2	output or transform plane.
r	distance from disturbance on the water surface.
R	radiant flux.
t	time.
$t(x_1, y_1)$	spacial light modulation function in P1 plane.
T	time duration of photographic exposure.
U	incident luminous flux.
V	velocity of ship or disturbance.
x,y	coordinates on the sea surface.
x_1, y_1	coordinates in P1.
x_2, y_2	coordinates in P2.
α_a	radius of aperture of class a.

β_o	incident angle.
γ	slope of D/logE curve in linear region.
Γ	reflectivity of sea surface.
δ	sea surface normal angle (angle between the normal and the zenith).
η	luminous efficiency.
θ_A, θ_B	normal angles (angle between ship's course and the direction of ship wave movement).
θ_c	critical angle.
λ	wavelength of light.
μ	angle between incident light wave and the zenith.
ρ	radial coordinate in P2.
σ	observer angle.
ϕ	phase.
Φ	wave slope energy spectrum.
ψ	angle between the observer-surface normal plane and the observer-zenith plane.
ω	radian frequency.
ω_x, ω_y	radian spacial frequency.

I. INTRODUCTION

A. BACKGROUND

Optical systems have received increased attention from physicists and engineers. The reason lies in the Fourier transform properties of a coherent optical system, and the laser has recently provided a practical source of coherent light. The optical image possesses two degrees of freedom (i.e.; the coordinates of a point on the surface) in contrast to the single degree of freedom, time, as found in electrical systems. With two degrees of freedom, an optical system appears to offer distinct advantages over an equivalent electrical system in some applications.

Since the electrical engineer is generally not familar with the Fourier properties of an optical lens, a brief description is presented here. More detailed analyses are given in Preston [1], Francon [2], and Goodman [3]. Consider the system diagrammed in Figure 1. The input plane, P1, is illuminated by a planar, unpolarized, unmodulated, monochromatic light wave described by the equation:

$$f_i(t) = f_o e^{j\omega t} \tag{1-1}$$

where ω is the radian frequency of the light wave. The plane, P1, contains a light modulator $t(x_1, y_1)$ such as a photographic transparency. The transmitted light is:

$$f_1(x_1, y_1, t) = f_o \bar{t}(x_1, y_1) e^{j\omega t} \tag{1-2}$$

where $\bar{t}$ is complex. Equation (1-2) may be written as:

$$f_1(x_1, y_1, t) = f_o t(x_1, y_1) \exp[j\omega t + \phi(x_1, y_1)] \tag{1-3}$$

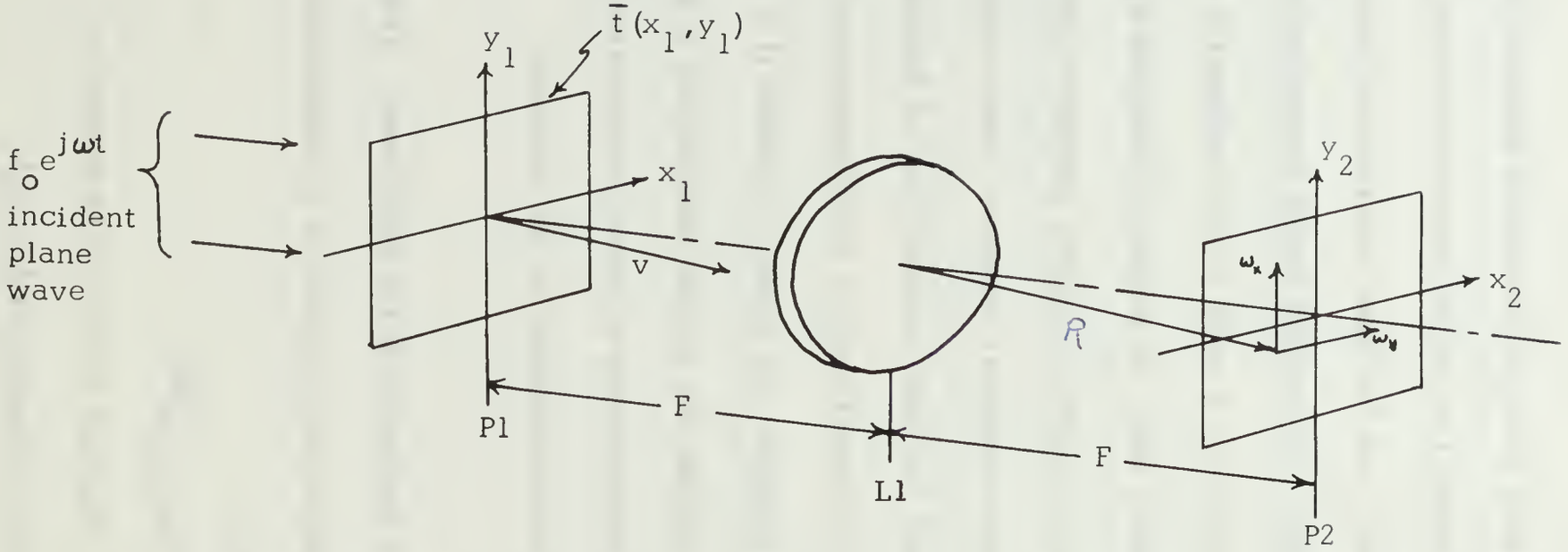

Figure 1. A single transform optical system.

Assume the lens to be ideal and the aperture, large so that vignetting does not occur. Geometric optics shows that the energy diffracted at P1 in the direction, v, will be summed at a point in the back focal plane, P2. It may be shown that the phase at the summing point, (x_2, y_2), is:

$$\phi(x_2, y_2) = \phi(x_1, y_1) + \frac{2\pi}{\lambda R}(x_1 x_2 + y_1 y_2) + \frac{2\pi d}{\lambda} \qquad (1\text{-}4)$$

where λ is the wavelength of light, R is shown in Figure 1, and d is the optical path length from the origin of P1 to the point (x_2, y_2). The light incident at the point, (x_2, y_2), becomes:

$$f_2(x_2, y_2, t) = f_o e^{j\omega t} \iint_{P1} t(x_1, y_1) \exp j\left[\phi(x_1, y_1) + \frac{2\pi}{\lambda R}(x_1 x_2 + y_1 y_2) + \frac{2\pi d}{\lambda}\right] dx_1 dy_1 \qquad (1\text{-}5)$$

The phase modulation term, $\phi(x_1, y_1)$, is usually made constant in practice and most often detection is by energy so the term outside the integral may be replaced by its rms value. For small diffraction angles where R is approximately equal to the focal length, F, equation (1-5) reduces to:

$$f_2(x_2, y_2) = f_m \iint_{P1} t(x_1, y_1) \exp j \frac{2\pi}{\lambda F}(x_1 x_2 + y_1 y_2) dx_1, dy_1 \qquad (1\text{-}6)$$

$$\text{where } f_m = \frac{f_o}{\sqrt{2}} \exp j\left[\phi(x_1, y_1) + \frac{2\pi d}{\lambda}\right]$$

Equation (1-6) is the two-dimensional, bounded, Fourier transform of the function, $t(x_1 y_1)$, multiplied by a system constant. This may be more readily apparent by rewriting the kernel function $\exp j(2\pi/\lambda F)(x_1 x_2 + y_1 y_2)$ as $\exp -j(\omega_x x_1 + \omega_y y_1)$ and defining:

$$\omega_x = -\frac{2\pi}{\lambda F} x_2$$

$$\omega_y = -\frac{2\pi}{\lambda F} y_2 \qquad (1\text{-}7)$$

Thus ω_x and ω_y are spacial frequencies defined in the back focal plane, P2. Two successive optical transform operations will map the input image into the output with only a coordinate reversal and a constant amplitude change.

B. APPLICATIONS

One of the more obvious applications follows directly from the above. Since the plane of the first transform, or frequency, plane displays the spatial frequency content of the input function, $t(x_1, y_1)$, frequency modifying operations such as band limiting and matched filtering may be performed in this plane. The theory is developed and some applications presented in Refs. 3 and 4.

By axis translation and successive transforming, other processes such as cross-correlation, auto-correlation, convolution, spectral analysis, and pattern analysis are possible. Many of these are discussed in Refs. 3, 5, and 6. Specifically such systems have found application in such diverse areas as character recognition [3 and 7], image improvement [8], synthetic aperture radar [9], and antenna simulation [6].

C. SCOPE OF THE THESIS

This thesis was conceived as a study of the merits of a low cost coherent optical processing system for student research. Although most systems in use perform two successive transforms, a single-transform system was considered more basic to the problem and such a system was constructed. Figure 2 is a photograph of the system. When completed,

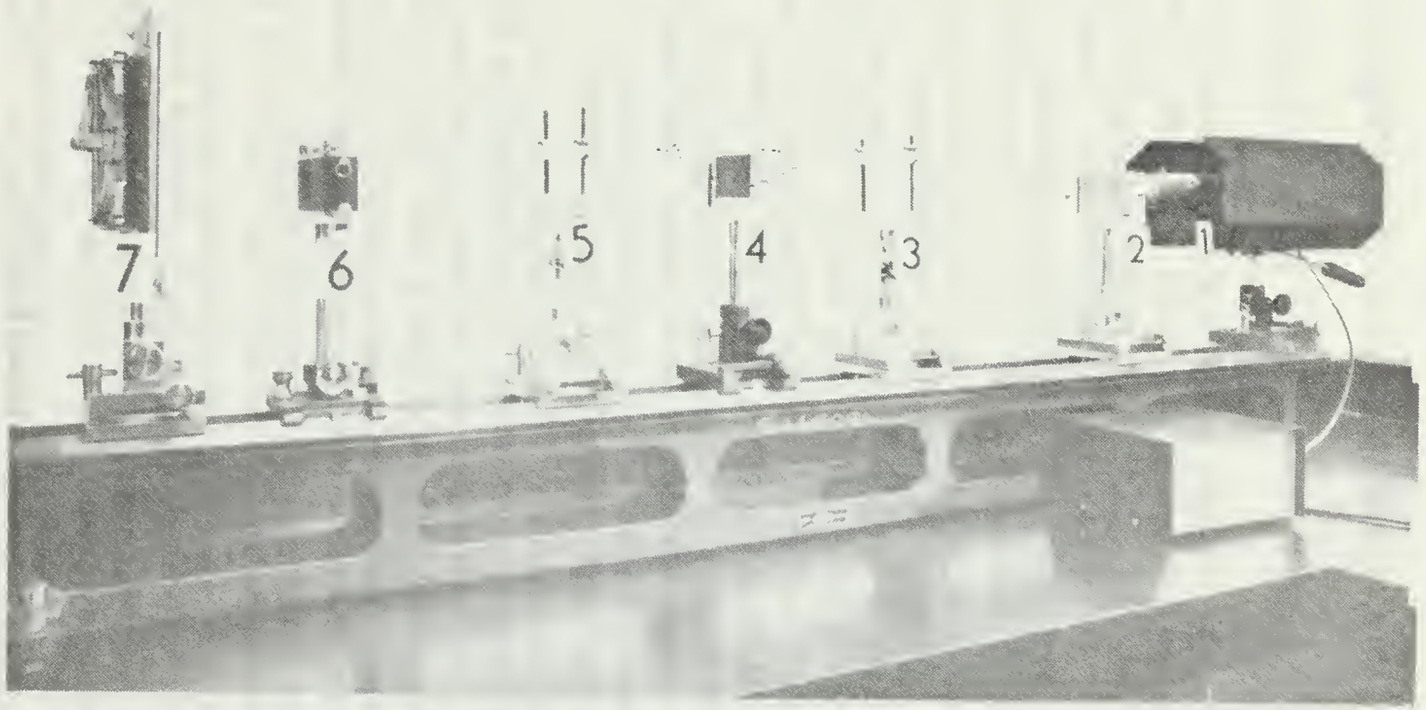

Figure 2. The experimental system. The noted components are: (1) 1.5mw He-Ne laser and condenser lens in a light baffle; (2) pinhole; (3) collimating lens; (4) the input plane; (5) the transform lens; (6) shutter; (7) output plane with film pack.

the system was used as a tool to investigate two otherwise unrelated topics. These topics were a study of film grain characteristics and a proposed method of ship detection via optical detection of the ship wave.

D. THESIS OUTLINE

Section II considers the effects of film in a single transform optical system. A model of the film grain is proposed and a statistical distribution of grain size is assumed. From this, a semi-quantitative mathematical prediction of the grain transform is developed. The grain size distribution of Polaroid Type 55P/N film was determined with photomicrographs and a prediction of the grain transform was made. The grain transform prediction was verified with an actual transform of a film specimen obtained with the constructed optical system.

A method of detecting ship waves is considered in section III. A relationship between light reflected from a ship wave to the camera and the optical transform of the resulting photograph was developed sufficiently to verify that a deterministic relationship does exist. A sample ship wave photograph was then operated on by a single Fourier transform with matched filtering in the frequency plane. The matched filter was rotated to investigate the possibilities of further electrical filtering of the frequency plane output.

Some suggestions for further research are given in section IV.

II. PROPERTIES OF FILM IN A SINGLE TRANSFORM SYSTEM

A. INTRODUCTION

Photographic film is the most commonly used medium for the input and output in an optical system. The primary advantage of film is its high information capacity which Jones [10] has compared with other media considered as information channels. The three film characteristics considered in this section may be thought of as disadvantages or limiting factors. The first factor is the time required to process the film, which in some cases may run several minutes both for the input and output. There are presently two means available to reduce this time; a Polaroid type film has a total processing time measured in seconds, while most conventional films can be processed in a specially prepared solution called a monobath which may require a few minutes. Based solely on time, the Polaroid type film seems the obvious choice. Although Polaroid negatives require clearing and emulsion hardening before use, the process could easily be mechanized and the time made very short. The Polaroid Type 55P/N film which provides both a positive and a negative was selected for evaluation in this project.

The two other limiting factors are the film's grain structure and its non-linear recording characteristics. These two factors were investigated in particular for Type 55 (negative) film, but the method is quite general.

B. A FILM GRAIN MODEL

Photographic films are generally constructed as shown in Figure 3. The process of exposing, developing, and fixing the film has the end result that the exposed grains are opaque and the unexposed grains have been washed from the film. This is described more fully by James and Higgins [11]. Even with no exposure, there are a certain minimum number of grains which will remain on the film as opaque spots. This, together with the density of the base, sets a minimum achievable density which is often referred to as fog level. The number of grains present increases as the exposure level increases and achieves a maximum density at some level dependent upon the particular film. Since this grain will be Fourier transformed and imaged along with the signal, its effect is of some importance.

The effects of grain have been treated in several papers such as Refs. 12, 13, and 14, where the grain is considered as noise having statistical properties. The problem is then one of a signal in the presence of noise and the techniques of communication theory are applicable. This treatment is ideally suited to double transform systems. However, this section is concerned with a single transform system, and the spatial frequency content of grain is of more interest.

A review of literature disclosed no appropriate model of film grain for a single transform. It became necessary to develop a model and test its validity in a single transform system. This model is developed in the following paragraphs and though it did not result in a completely mathematical expression, the result is seen to be of value.

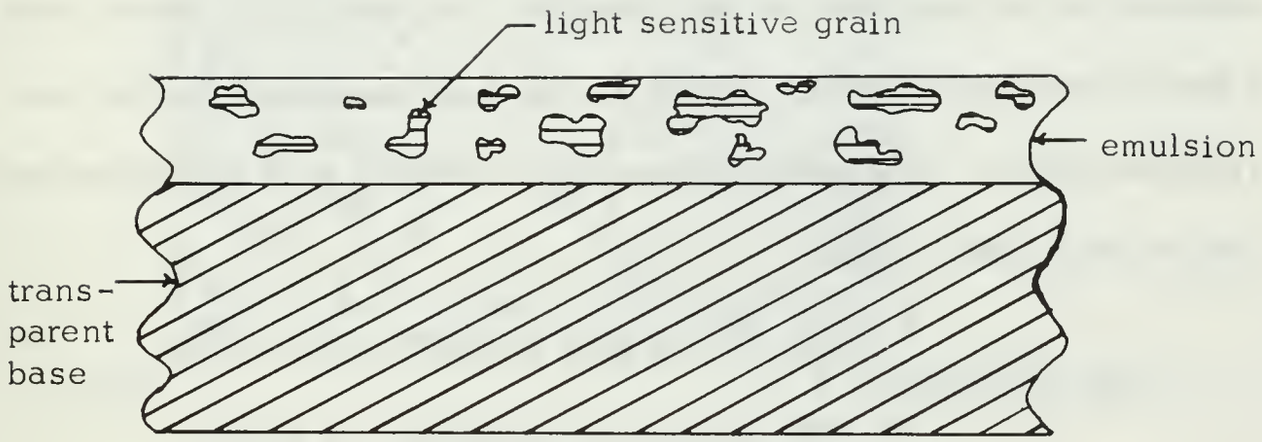

Figure 3. Cross-section of a negative film.

Figure 4 is a photomicrograph of Type 55 (negative) film with no exposure. The density is thus D_{min} which is specified 0.18. The photograph suggested a grain structure model of overlapping circular stops. Since the diffraction pattern due to apertures distributed identically to the stops will be essentially the same, the model is initially composed of apertures which is mathematically easier to handle.

Francon [2] considered the Fourier transform of several apertures identical in shape. The model based on Figure 4 is composed of circular apertures of varying size but with the size-frequency distribution constant. A grain class was defined as a set of grains (or apertures) having one specified radius. The work of Francon may now be used to find the transform of each class. Thus:

$$f_a(x_2, y_2) = f(x_2, y_2)_a \sum_{n=1}^{N_a} e^{j\frac{k}{F}(x_2 x_{1n} + y_2 y_{1n})} \qquad (2-1)$$

where N_a is the total number of grains in class a, $f(x_2, y_2)_a$ is the Fourier transform of one aperture of class a, $f_a(x_2, y_2)$ is the Fourier transform of the set called class a, k equals $2\pi/\lambda$, and F is the transforming lens focal length. In words, the output due to the set of apertures in class a is the summation of N_a outputs, each identical in magnitude but of varying phase. The total output of a given area of film becomes the summation over the area of all grain classes.

$$f_T(x_2, y_2) = \sum_{a=1}^{a_T} f_a(x_2, y_2) \qquad (2-2)$$

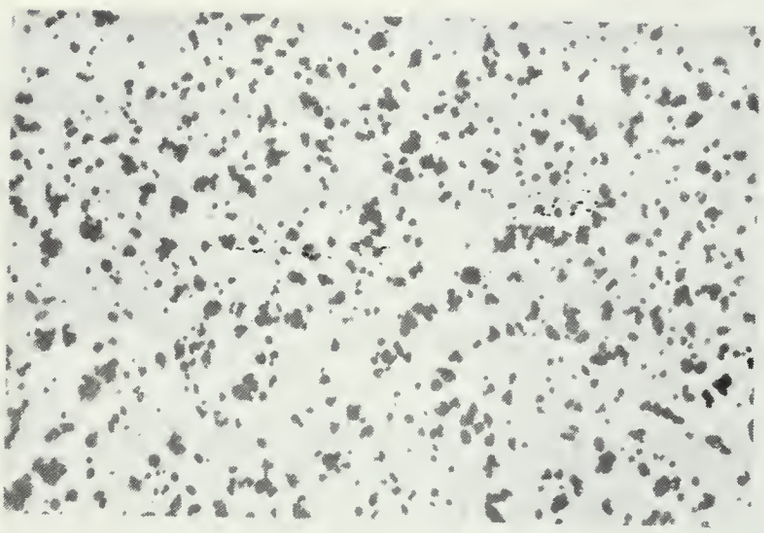

Figure 4. Photograph of Polaroid Type 55 (negative) film with no exposure. (1000X).

where a_T is the total number of classes, and $f_T(x_2, y_2)$ is the total Fourier transform. The intensity in the transform plane is:

$$I_p = |f_T(x_2, y_2)|^2$$

$$= \left| \sum_{a=1}^{a_T} \left[f(x_2, y_2)_a \sum_{n=1}^{N_a} e^{j \frac{k}{F}(x_2 x_{1n} + y_2 y_{1n})} \right] \right|^2 \qquad (2\text{-}3)$$

$$= \sum_{a=1}^{a_T} \left\{ f^2(x_2, y_2)_a \sum_{n=1}^{N_a} \sum_{m=1}^{N_a} e^{j \frac{k}{F}\left[x_2(x_{1n} - x_{1m}) + y_2(y_{1n} - y_{1m}\right]} \right\}$$

For N_a large, there are a large number of sine and cosine terms, the sum of which goes to zero except when m=n. Thus, this term sums to N_a and,

$$I_p = \sum_{a=1}^{a_j} \left[f^2(x_2, y_2)_a \, N_a \right] \qquad (2\text{-}4)$$

But this is not the complete story. From equation (2-3), the intensity at the x_2, y_2 origin is:

$$I_p = \sum_{a=1}^{a_T} \left[f^2(x_2, y_2)_a \sum_{h=1}^{N_a} \sum_{m=1}^{N_a} 1 \right] = \sum_{a=1}^{a_T} \left[f^2(x_2, y_2)_a \, N_a^2 \right] \qquad (2\text{-}5)$$

The intensity at the origin is a function of the square of the number of grains rather than the number of grains as in equation (2-4). Francon [2] indicates that, for equal apertures, experiment shows this bright central region to be surrounded by a dark ring. Since there are a large number of apertures in a limited surface, there is necessarily a certain distribution of separation between each grain and its nearest neighbors which is not entirely random. The resulting order in the separations produces this dark ring. In the same reference, Francon shows that the remainder of the output is granular in appearance since the intensity deviation due

to the phase terms is of the same order as the mean. This effect is noted in many other papers and is the cause of the granular appearance which is characteristic of coherent illumination.

The transform of a single circular aperture was then considered. This is covered in some detail by Goodman [3] and is:

$$f(x_2, y_2)_a = \mathcal{F}[\text{circ}(\alpha_a)] = (\pi \alpha_a)^2 \left[\frac{2J_1(Z)}{Z}\right] f_o \qquad (2\text{-}6)$$

where α_a is the radius of apertures in class a, $J_1(Z)$ is the first-order Bessel function, and f_o is the incident light function (a constant). The other terms are defined as follows:

$$\text{circ}(\alpha_a) = \begin{cases} 1 & \text{for } x_1^2 + y_1^2 \leq \alpha_a \\ 0 & \text{elsewhere} \end{cases}$$

$$Z = \frac{2\pi}{\lambda F} \alpha_a \rho \qquad (\rho^2 = x_2^2 + y_2^2)$$

(This function has circular symmetry about the optical axis and is sketched in cross-section in Figure 5). The intensity distribution due to one aperture is the square of the function in Figure 5. Figure 6 is the transform of a 100 micron radius aperture and was obtained with the experimental system described later. From equation (2-5), the expression for intensity now becomes:

$$I_p = I_o \sum_{a=1}^{a_T} N_a \pi^2 \alpha_a^4 \left[\frac{2J_1(Z)}{Z}\right]^2 \qquad (2\text{-}7)$$

This neglects the central region and the granularity effects.

The original intent was to follow this line of analysis to find an expression for the total transform with the size-frequency distribution of

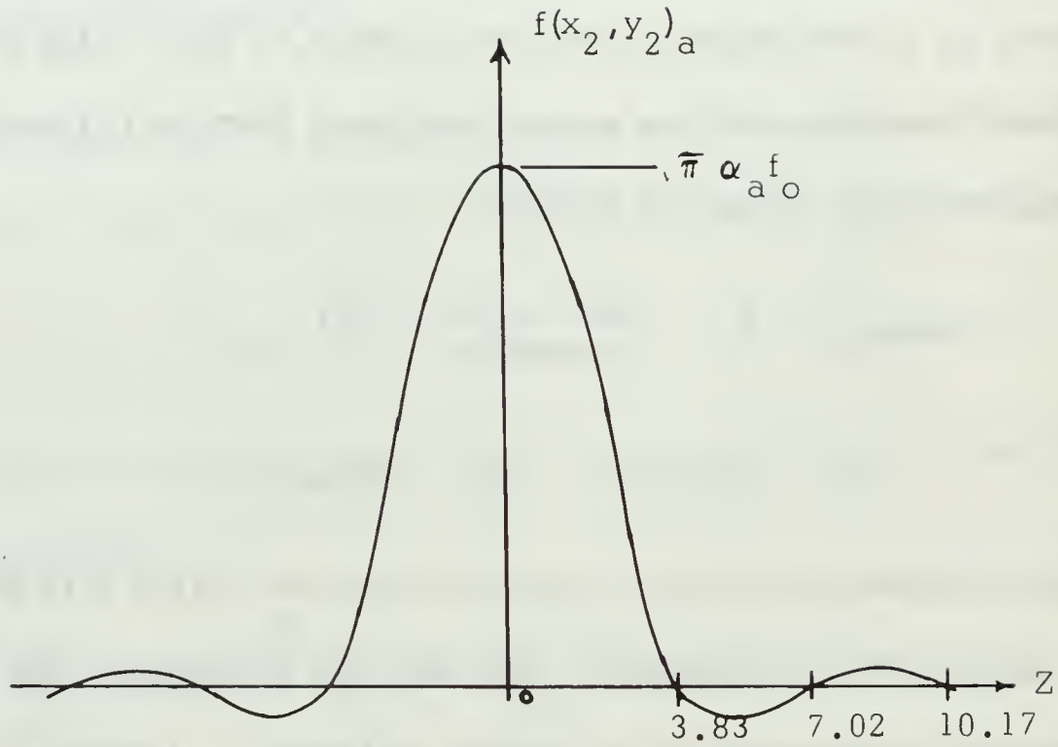

Figure 5. The first-order Bessel function.

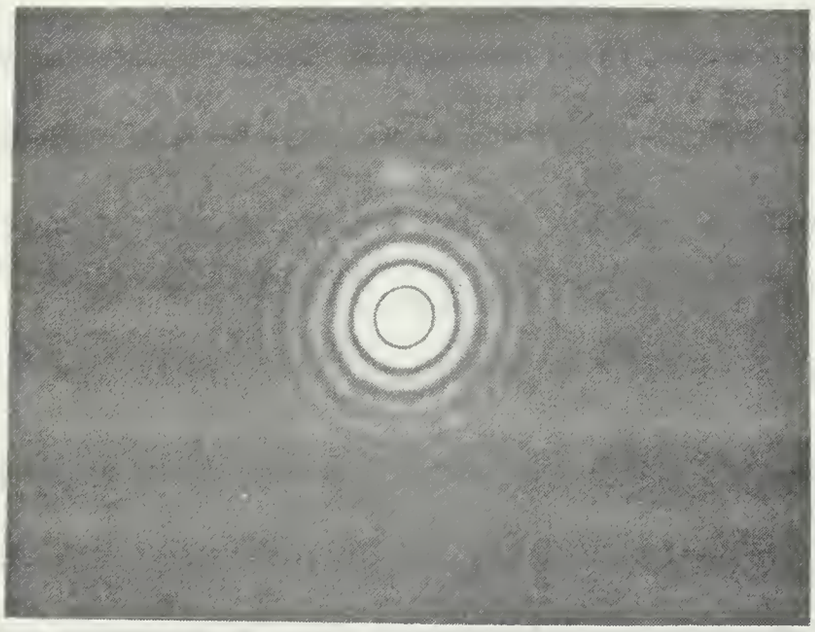

Figure 6. Fourier transform of a 100 micron radius aperture. (focal length=50cm).

α_a known. However, this involves the distribution function of the output which is obtained by finding the inverse of the term $2J_1(Z)/Z$. No practical method of obtaining the inverse was found. The output can be obtained rather easily, though, for a finite number of classes by graphical summation. This was the technique used to complete the analysis.

Up to this point, circular apertures have been considered, whereas the grain structure model involves circular stops. Defining f_{2S} as the transform due to a circular stop model, f_{2a} as the transform due to a circular aperture model, and f_o as the transform of the incident light (source light), the following relationship applies:

$$f_{2S}(x_2, y_2) = f_o(x_2, y_2) - f_{2a}(x_2, y_2) \qquad (2-8)$$

The function $f_o(x_2, y_2)$ will be the transform of a circular aperture defined by the system's limiting aperture. This is generally the beam size itself, and since it is large compared to a grain size, the pattern f_o will be confined to the region near the origin. At a small distance from the origin, only f_{2a} and f_{2S} are significant and:

$$f_{2S}(x_2, y_2) = - f_{2a}(x_2, y_2) \qquad (2-9)$$

or:

$$f_{2S}^2(x_2, y_2) = f_{2a}^2(x_2, y_2) \qquad (2-10)$$

That is to say that the intensity distribution of the transforms of complementary inputs are identical except at the origin. This is Babinet's Complementary Aperture Theorem [2].

Considering all of the above factors, the film grain transform will exhibit a brilliant spot at the origin due to the function $f_o(x_2, y_2)$ (in

effect - the DC term), and the N_a^2 factor of equation (2-5). Surrounding this is a dark annular ring as noted above. The remainder of the pattern will be granular in appearance with a mean distribution given by equation (2-7).

Thus far this analysis has ignored the fact that the film thickness varies. Although some variations will occur solely because of manufacturing tolerances, the most prominent effect is due to the processing action of exposed grain removal [3]. By defining $\phi_n(x_{1n}, y_{1n})$ to be the additional phase introduced at each grain center, equation (2-1) becomes:

$$f_a(x_2,y_2)=f(x_2,y_2)_a \sum_{n=1}^{N_a} e^{j\left[\frac{k}{F}(x_2x_{1n}+y_2y_{1n}) + \phi_n\right]} \qquad (2\text{-}11)$$

The analysis then follows as before with a similar result. The output pattern is essentially the same as given in equations (2-4), (2-5), and (2-7) except near the origin. Note that for $x_2=y_2=0$, ϕ is not necessarily equal to zero, and some of the intensity at the origin must be dispersed over a slightly larger area. The dark ring surrounding the origin will not necessarily be at the same radius since the causal order depends on both the grain-center separations and the emulsion thickness variations.

C. THE PREDICTED TRANSFORM RELATED TO FILM DENSITY

A size-frequency distribution was obtained from Figure 4 and the results given in Table I and Figure 7. A size count such as this is somewhat arbitrary and very dependent on the judgement of the observer. The guidelines used were: (1) for clumps of more than one grain, choose the

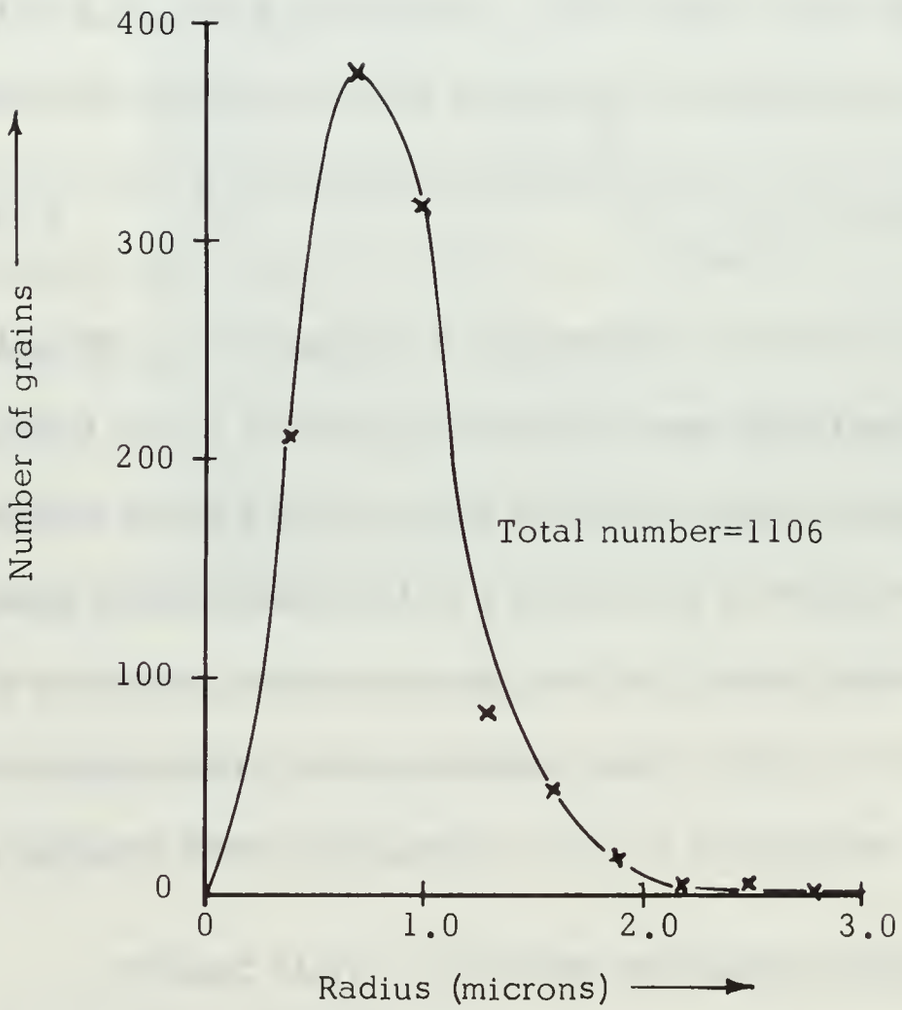

Figure 7. Size-frequency curve of Polaroid Type 55 (negative) grain.

TABLE I. GRAIN SIZE COUNT.

Class Diameter	Diameter Range	Number	Weight (number/total)
0.4μ	0.3-0.5μ	259	.234
0.7	0.6-0.8	377	.341
1.0	0.9-1.1	315	.285
1.3	1.2-1.4	84	.076
1.6	1.5-1.7	47	.042
1.9	1.8-2.0	15	.014
2.2	2.1-2.3	4	.004
2.5	2.4-2.6	5	.005
2.8+	2.7- ∞	0	.000
	Total	1106	1.001

largest sub-units which could be considered as circular and count each as one grain, (2) whenever possible, choose sub-units such that overlap is minimized. The resulting curve of Figure 7 is similar to a typical curve given in Ref. 11.

The data of Table I was used to determine the intensity distribution in accordance with equation (2-7). Figure 8 is a plot of the transforms of each size-class and the total transform. There are no sharply defined nulls or peaks in the total transform which was to be expected since this is the transform of a continuously distributed input. The curve is a smoothly decreasing function of radius, which is difficult to study by experiment without some means of accurate light intensity measurement. Photographic film does not supply the desired accuracy and, at this time, no other means was available. At this point, it seems worth mentioning that the transforms of many signals of interest are not continuous spectra. As such their patterns will approach point spectra which are more easily

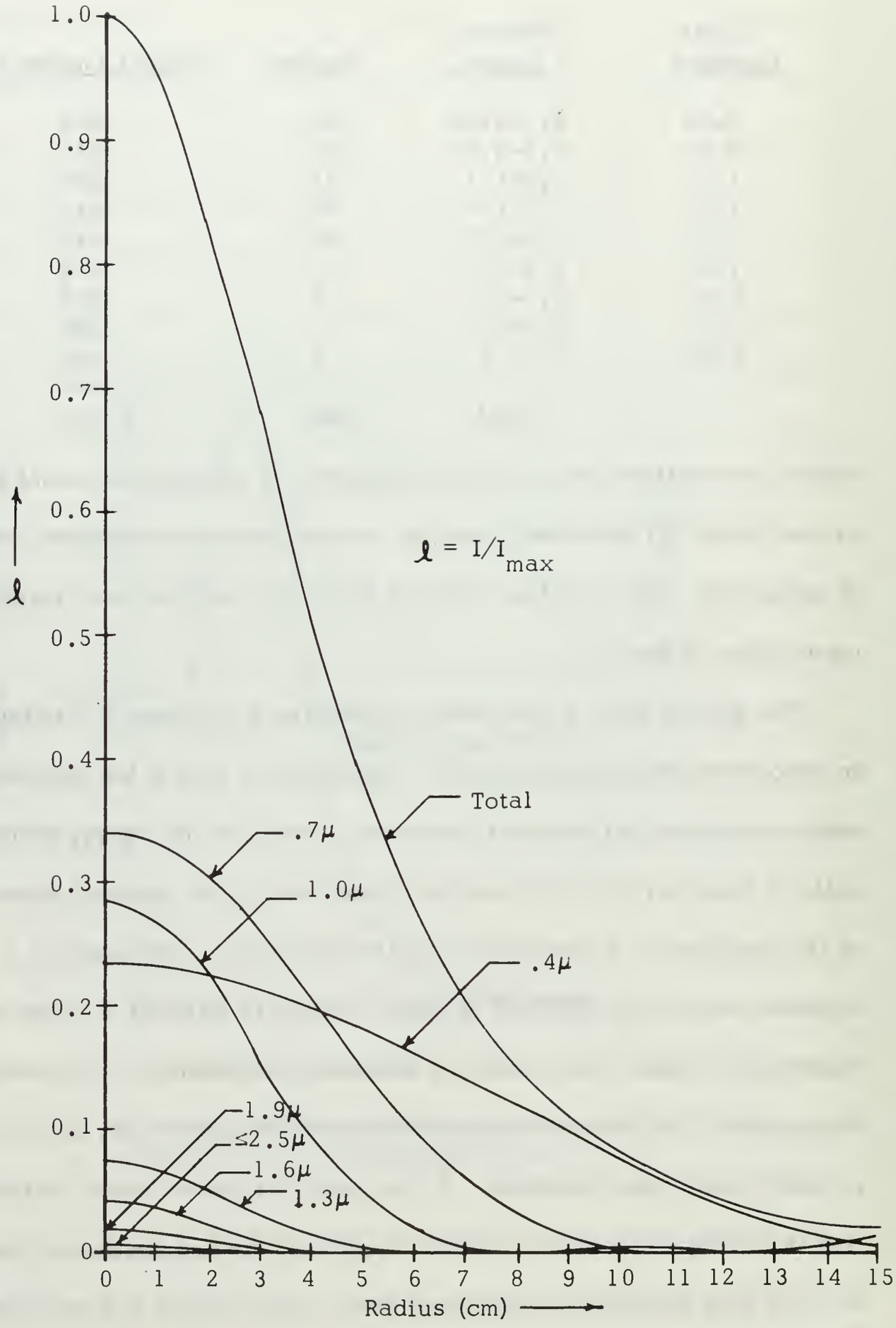

Figure 8. Fourier transform of Type 55 (negative) film grain by graphical summation. (focal length=10 cm).

analyzed. Film can provide only a rough quantitative analysis for the continuous distributions as in the present case.

Type 55 (negative) film was chosen for the output medium. The D/logE curve (see Appendix A) is non-linear except in the central region of the slope. This is generally true of any film. In the linear region, the following relation holds:

$$D = \gamma \log E + \text{constant}$$
$$= \gamma \log IT + \text{constant} \qquad (2\text{-}12)$$

where E is the photographic exposure, and T is the time duration of the exposure. This relation is valid from D=0.375 to 1.5. The range of output intensities far exceeded the linear range of the film and many exposures were needed at various values of T to cover the range. Thus, by considering the linear density regions of output films exposed at various values of T, the effective linear density range was extended. Since the intensity at a given radius must be a constant for all photographs, two successive photographs were compared by letting:

$$\Delta D = \gamma \log \frac{I_1 T_1}{I_2 T_2}$$

and set $I_1=I_2$. Thus:

$$\Delta D = \gamma \log \frac{T_1}{T_2} \qquad (2\text{-}13)$$

In practice, a ΔD was determined by comparing densities at equal radii in two photographs.

D. THE GRAIN TRANSFORM BY EXPERIMENT

The optical system for this experiment is diagrammed in Figure 9. The position of L_1 and P_1 are reversed compared to the normal arrangement, which alters the transform kernal from $\exp(jk/F)\ (x_1x_2+y_1y_2)$ to $\exp(jk/d_1)\ (x_1x_2+y_1y_2)$ and offers some control over the size of the output [3]. The input no-exposure transparency was placed against an optical flat with a matching fluid (mineral oil) between the two. Several exposures of the transform were taken to cover the intensity range with the input transparency base side against the fluid. A similar set of exposures was made with the emulsion side against the fluid. A single exposure was taken with the input transparency unmatched by the fluid. A visual comparison was made with the single unmatched output and the two matched cases at the same exposure level. The case with the fluid against the film base appeared virtually identical in density to the unmatched case, indicating that the base thickness variations have a negligible effect for this film. The emulsion-matched set of exposures correspond to equation (2-7) with no random phase variations. The base-matched set of exposures correspond to equation (2-11) because of the phase variations due to the unmatched emulsion side.

The density of each of the exposures was recorded using a microdensitometer to track a diametric line through the origin. Figures 10 and 11 are typical density recordings from each of the sets. Figures 12 and 13 are the corresponding Type 55 positives for these two recordings.

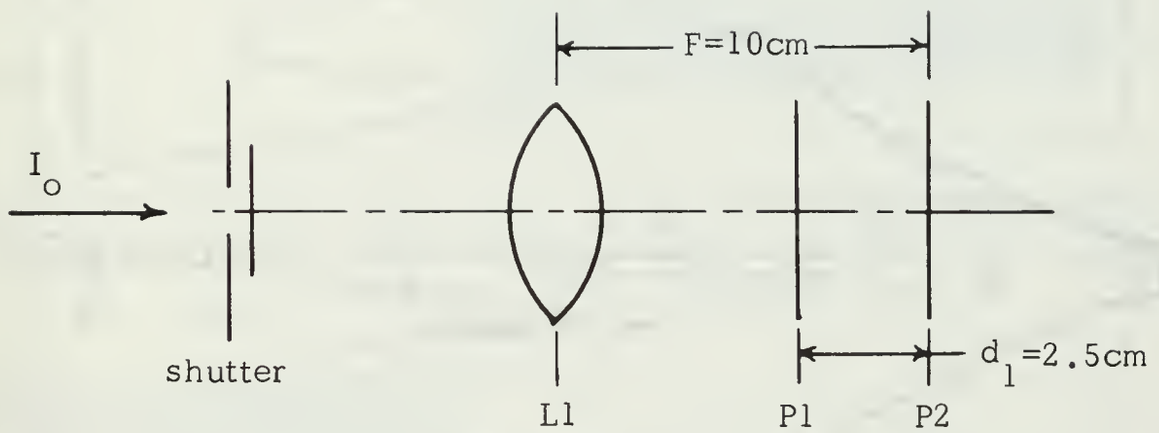

Figure 9. Optical system for grain structure Fourier transform.

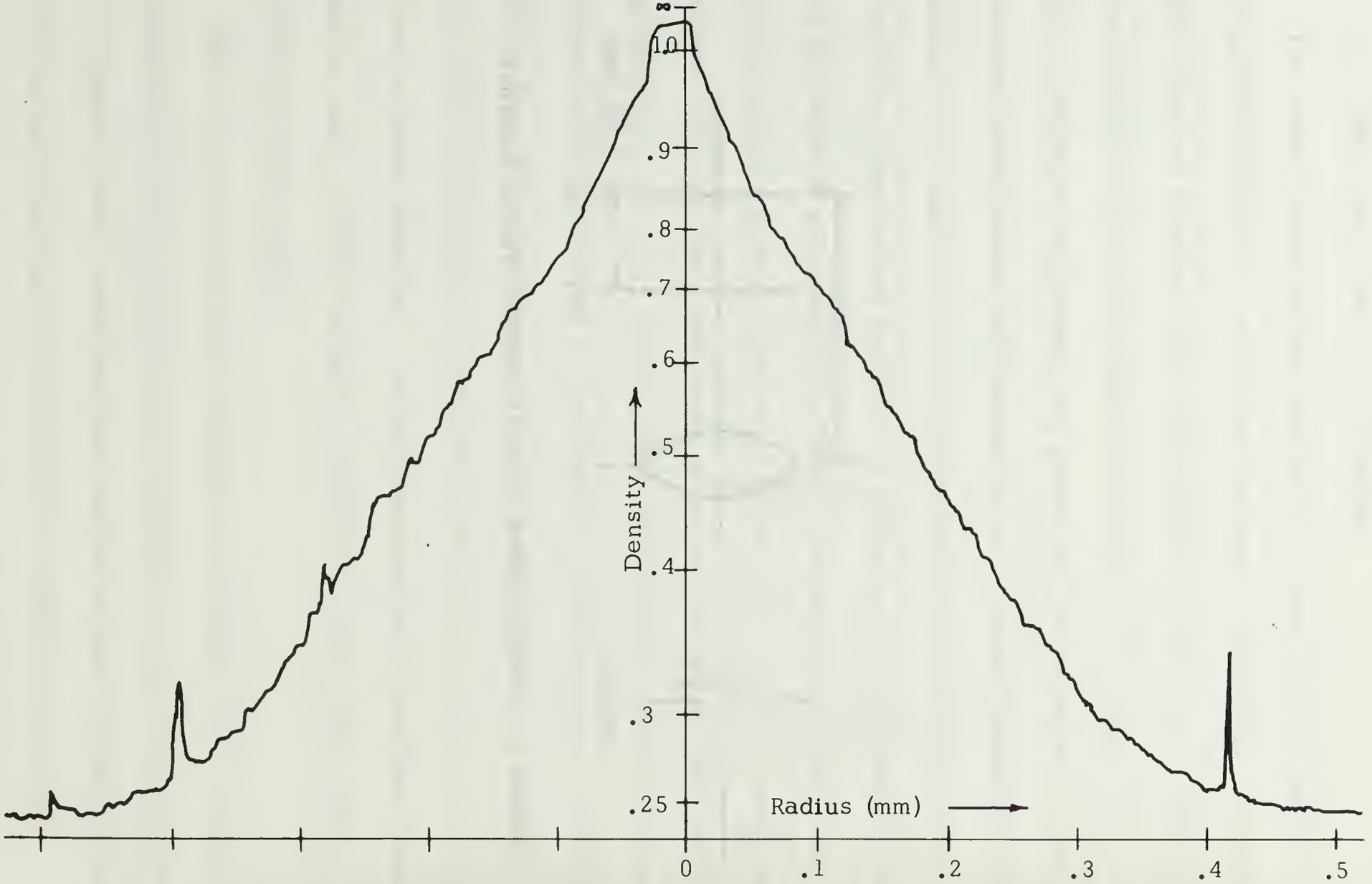

Figure 10. Microdensitometer recording of Type 55 (negative) film grain transform with emulsion surface fluid matched.

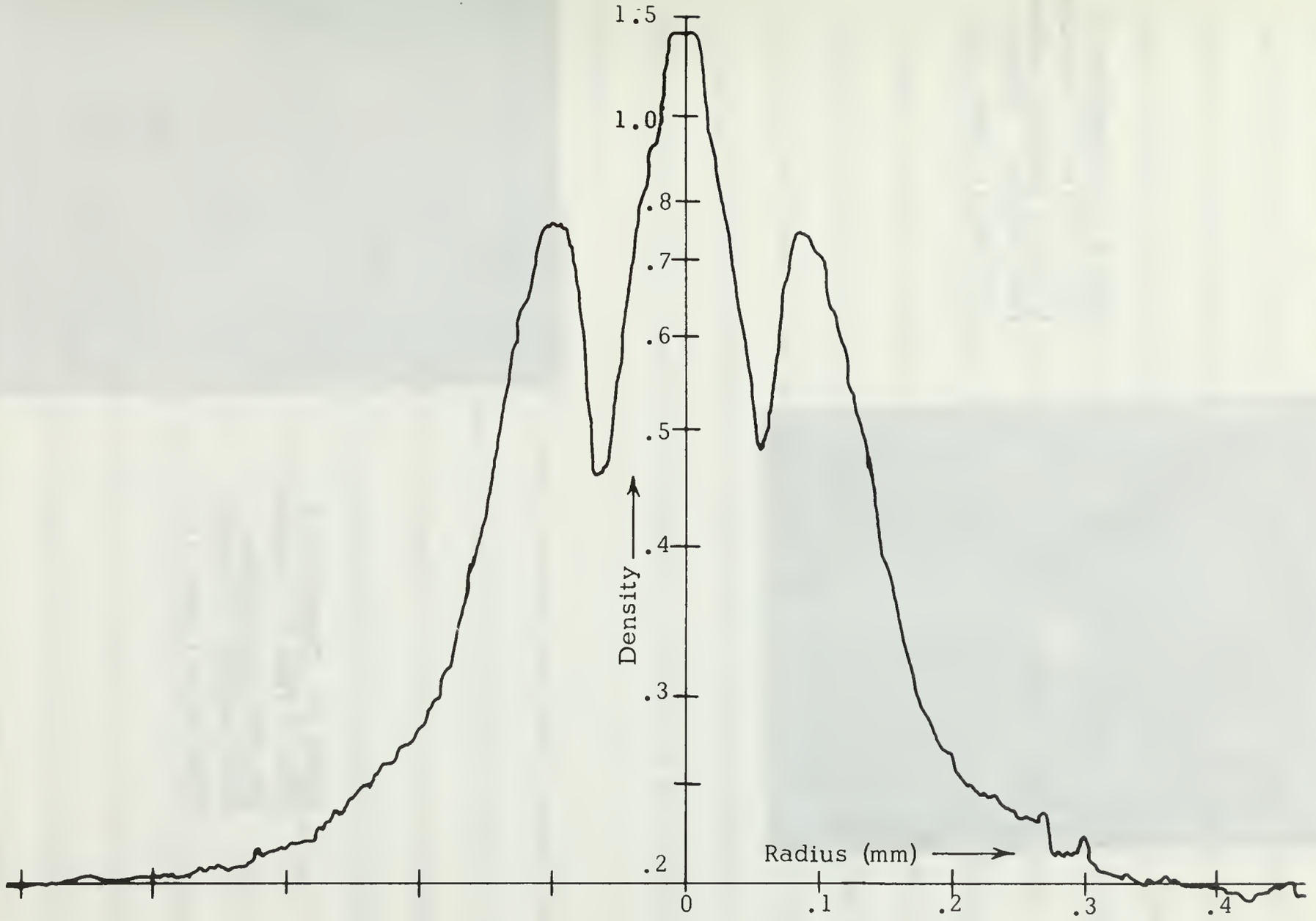

Figure 11. Microdensitometer recording of Type 55 (negative) film grain transform with base surface fluid matched.

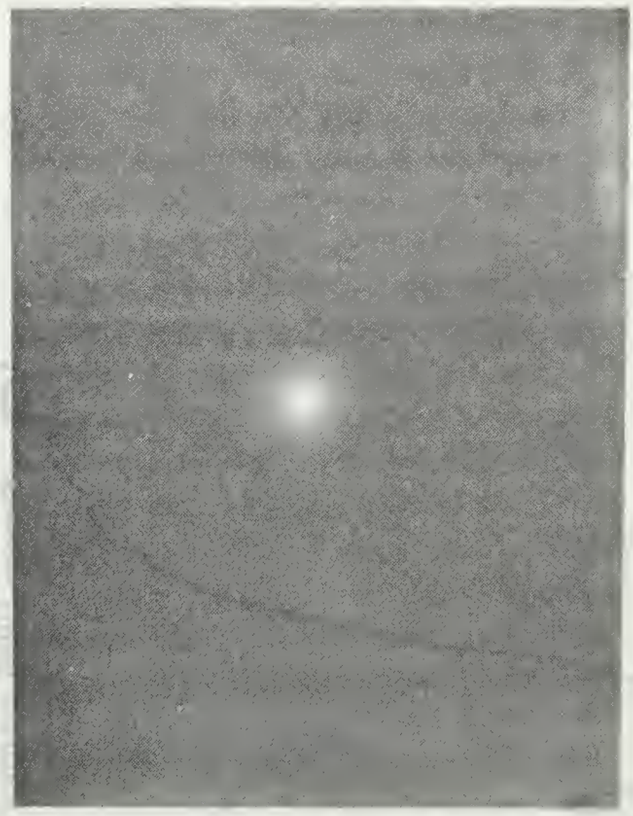

Figure 12. Transform of grain in Type 55 (negative) film with emulsion surface fluid matched. (Density recording is Figure 10).

Figure 13. Transform of grain in Type 55 (negative) film with base surface fluid matched. (Density recording is Figure 11).

The exposure level is not the same for these two photographs and no comparison of the exact density levels should be made. They are presented here only as typical of each set. In both figures, the peak is in saturation while the minimum level is below D_{min}. The bright central peak and dark annular ring are obvious in Figures 11 and 13. In Figure 12, a faint ring is visible at a larger radius and appears as two spikes in Figure 10. Although this ring may also be due to the non-random order of apertures separated by short distances, it would be impossible to verify it without further knowledge of the film construction. A fine structure is evident in the recordings but the true character of granularity cannot by recorded by the microdensitometer since the variations occur in the order of one wavelength (0.6328 microns). The "tailing-off" in both figures is due to the film non-linearity in the toe of the D/logE curve.

The series of exposures in each set were compared in density as noted above. The resulting density curves are plotted in Figure 14. The theoretical curve of Figure 8 was converted to density levels and also plotted in Figure 14. Note that the theoretical curve was derived from equation (2-7) which does not consider the effects near the origin. It must also be in error due to the effect of overlapping grains. When the grains overlap, the resulting shape is no longer circular and the dimension in one direction becomes much larger on the order of multiples of the smaller dimensions. Referring to Figure 8, note that the transforms of the larger grains affect the resulting curves at low values of radius. The

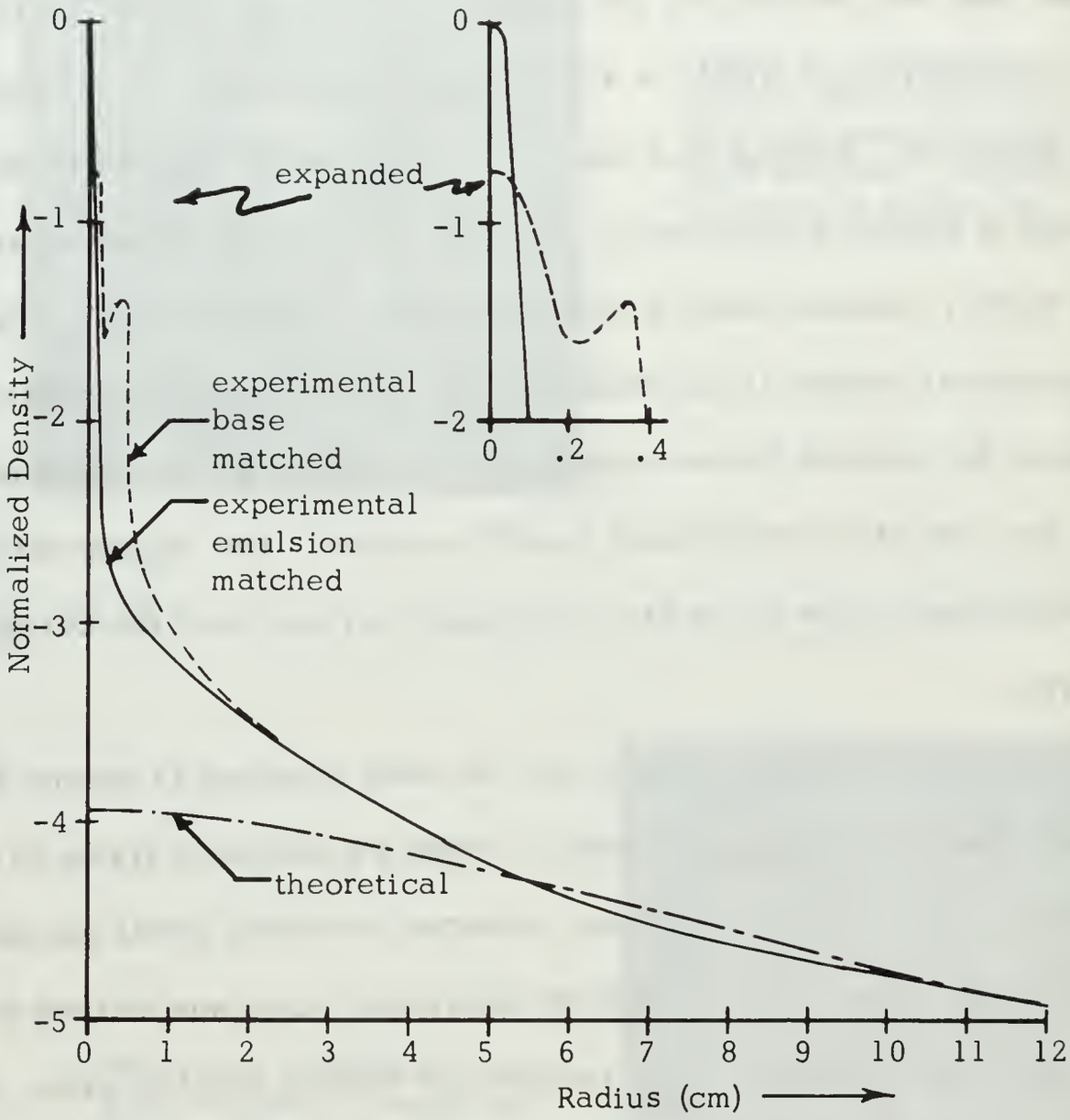

Figure 14. Normalized Fourier transform curves for Type 55 (negative) film grain. Density levels based on a linear D/logE characteristic using Type 55 (negative) to record the output. (focal length=10cm).

small grain transforms have a proportionately greater effect at large radii. The photomicrograph of Figure 4 shows very little overlapping for the smaller grains, keeping in mind the judgement criteria upon which the grain count was based. Thus, the experimental results at large radii should closely approximate theory. The curves of Figure 14 were normalized by equating the density levels at a radius of 12 cm.

The experimental and theoretical curves show excellent agreement between 5 and 12 cm radius. There is no reason to believe that they would not continue to agree at larger radii but the curve could not be extended further because of lens curvature of field. The density departed from the theoretical curve for small radii in the manner predicted. That is, the intensity was higher near the origin due to the strong DC term and the effects of overlapping. It was noted also that the peak of the base-matched curve was less than for the emulsion-matched curve and that the intensity was somewhat more dispersed about the origin.

The method of this section has been both quantitative and qualitative. Exact agreement between theory and experiment is not possible because the model is not an exact copy of the true grain structure. Had a better means of determining the intensity distribution been available, the normalizing procedures would not have been necessary and the results would, admittedly, carry more validity. However, the close agreement which does exist between theory and experiment is sufficiently convincing to prove the essential correctness of the model.

E. THE SIGNAL-PLUS-GRAIN TRANSPARENCY

Thus far only the transform of the minimum grain level has been considered. This must now be related to a transparency composed of this minimum grain density with a signal superimposed on it. A typical transparency may consist of a continuous distribution of densities or a set of binary density levels, D_{max} and D_{min}, but in either case the signal is on a background field of D_{min} or D_{max}. Since there exists a limited density range, the signal itself must consist of some grain structure even in the binary case.

Figures 15 and 16 are photomicrographs of Type 55 (negative) film with density levels greater than D_{min} and they should be compared with Figure 4. It is obvious from Figure 14 that the circular grain model is far less representative of the actual grain structure when the grain structure is composed of irregular clumps. The nature of the exposure-development process is not fully understood, though several plausible theories have been proposed [11]. It is important here to note only that a clumping effect does occur and that it increases with density. Larger dimensions are now involved and, from the previous discussion in the effect of increased dimensions, an increase in intensity near the origin occurs at the cost of intensity at large radii. Assuming the input transparency area to be large compared to the size of any one grain, the size distribution is identical in all directions, and the output transform due to grain will still be symmetrical about the origin. The central DC term is reduced at the same time due to the overall increase in density.

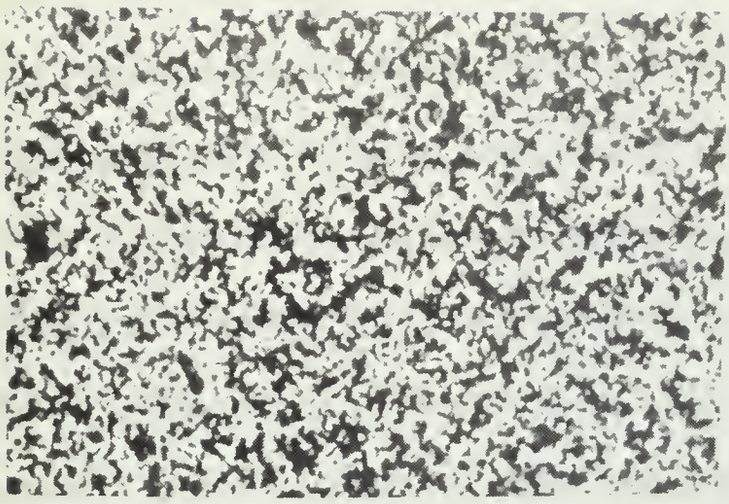

Figure 15. Photomicrograph of Type 55 (negative) film. Density 0.7.

Figure 16. Photomicrograph of Type 55 (negative) film. Density 1.7.

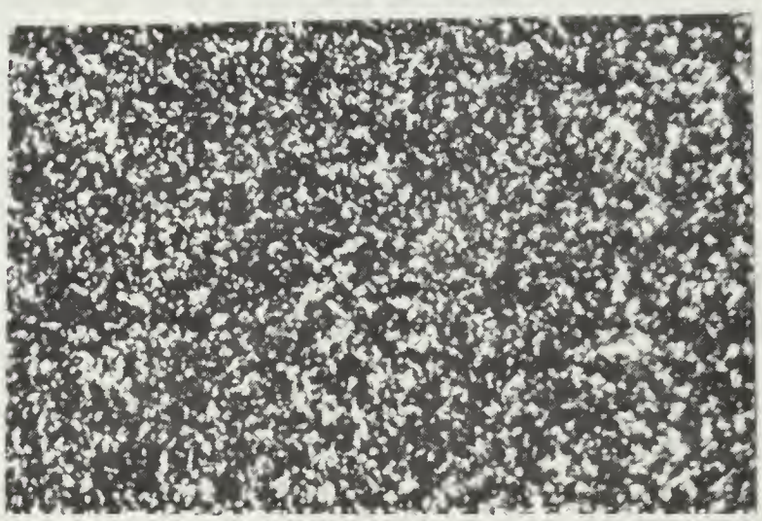

The shifting of energy to smaller radii due to larger grain dimensions continues until the total grain area of the negative is approximately equal to the transparent area. Further increases in exposure produce negatives whose grain structure is approximately the complement of that for the negatives with lower densities. That is, the structure is one of transparent apertures rather than opaque stops. Indeed, in Figure 16, the structure appears to be a rough complement of Figure 4. The Complementary Aperture Theorem of Babinet predicts identical diffraction patterns for complementary screens except for the central DC term. Exact complements cannot be expected because the apertures of the high density negatives do not have the circular structure of the stops of the low density negatives. For these structures, an increase in density results in a shift of energy in the transform from small to large radii. The central DC term continues to decrease.

A signal transparency will contain more than one density level and the output transform due to the grain alone will be dependent on the existing input density levels and relative areas which they occupy. The binary input consists of areas of complementary grain structures and the output will be the signal transform plus a grain transform which approaches that in Figure 8 or 12. The worst case occurs when the input consists of intermediate densities where the grain size is about equal to the aperture (between grain) size. The transform intensities are more dispersed.

Returning to Figure 14 and remembering that photographic film has a limited recording range (ΔD is about 1.5 for Type 55), it is seen that an adjustment of exposure level to place the tail of the curve below D_{min}

leaves only the grain transform near the origin. The effect of grain (with the emulsion matched) in the transform would be a central disc on the order of 0.2 cm radius for a focal length of 10 cm or, in general, 0.02X (focal length in cm) for Type 55 (negative) film. This means that the signal can have no significant frequency content less than about 2×10^3 cycles/cm for this film.

Figures 17, 18, and 19 are a series of signal transforms which were designed to test the above hypothesis and serve as a visual demonstration of transforms in the presence of grain. In practice, the best output was obtained at an exposure level which included some of the tail of the density curve of Figure 14. Figure 17 is the transform of D_{min} grain alone. The signal input for Figures 18 and 19 were 2mm high characters with density D_{min} against a field of D_{max}. The fine structure of concentric rings seen in all three photographs is due to a small aperture mask required to select a particular character on the input transparency. Although the grain transform does degrade the image, the distinguishing features of the signal transforms are readily apparent.

F. CONCLUSIONS

Although the experimental grain transform differed significantly from the theoretical grain transform, the essential correctness of the grain model was verified. The overall effect of the grain appeared as a reduction in bandwidth by setting a lower limit of useful frequency response in cycles/cm. This effect appears to contradict intuition since grain is

Figure 17. Transform of film grain. Exposure is the same as for Figures 18 and 19. (focal length is 50 cm).

Figure 18. Transform of the character '4' in the presence of film grain. (focal length is 50 cm).

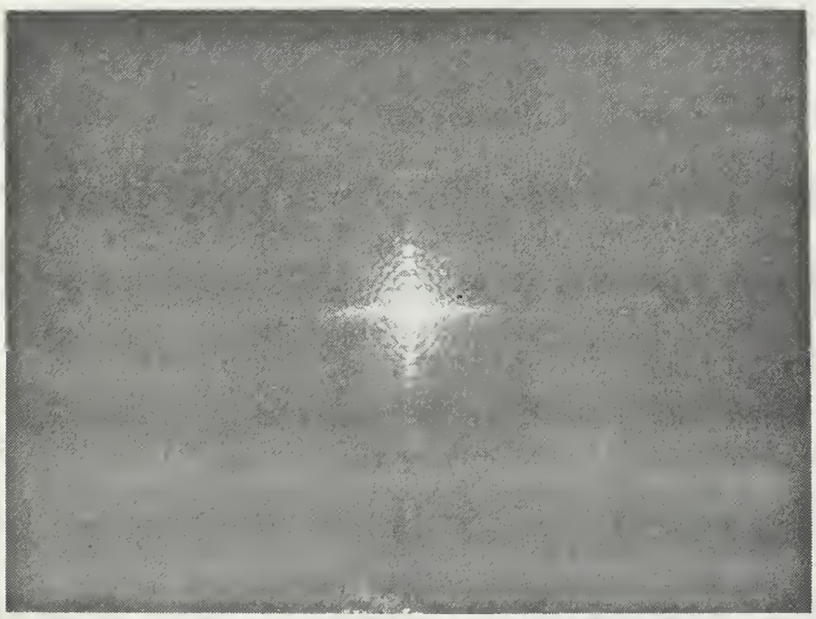

Figure 19. Transform of the character '5' in the presence of film grain. (focal length is 50 cm).

usually thought of in terms of limiting the fine detail, or the high spatial frequencies in an image. However, the following discussion shows that this is a special case and the results are somewhat misleading because a relatively grainy film was used.

It must be noted that no part of the signal, including the fine detail, can have dimensions less than the diameter of the smallest grain. In most cases, the lowest spatial frequency of even the finest detail in the signal will fall in the central region where the grain transform is significant. The higher frequencies of the signal are visible here only because the signal transform intensity is significantly greater than the grain transform intensity in this frequency range. As seen earlier, the total intensity of the grain transform is a function of the total number of grains (or apertures in the case of D_{max}) in the input transparency. The grain transform intensity was reduced by limiting the area of the input transparency to include little more than the signal area as in Figures 17, 18, and 19. Retention of the low frequency signal spectrum, including that in the fine detail would require that the signal transform intensity be greater than the transform intensity over the range of the signal bandwidth. Extremely fine grain films are required to disperse the grain transform spectrum and "flatten" the curve of Figure 8.

Consider a limiting case, shown in Figure 20, in which the grain transform is so dispersed that it appears essentially constant over the spatial frequency bandwidth of the signal. In a typical signal, the transform intensity would be a decreasing function of frequency. Above

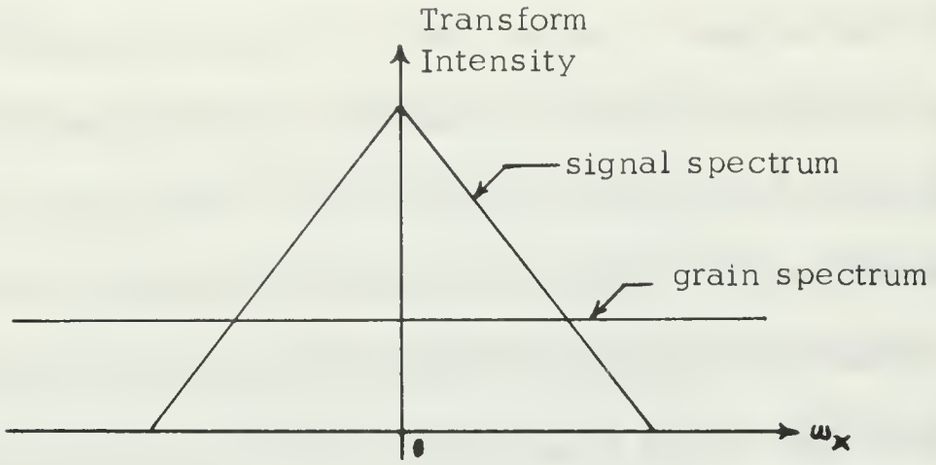

Figure 20. Idealized signal and grain spectrums for a signal on fine grain film.

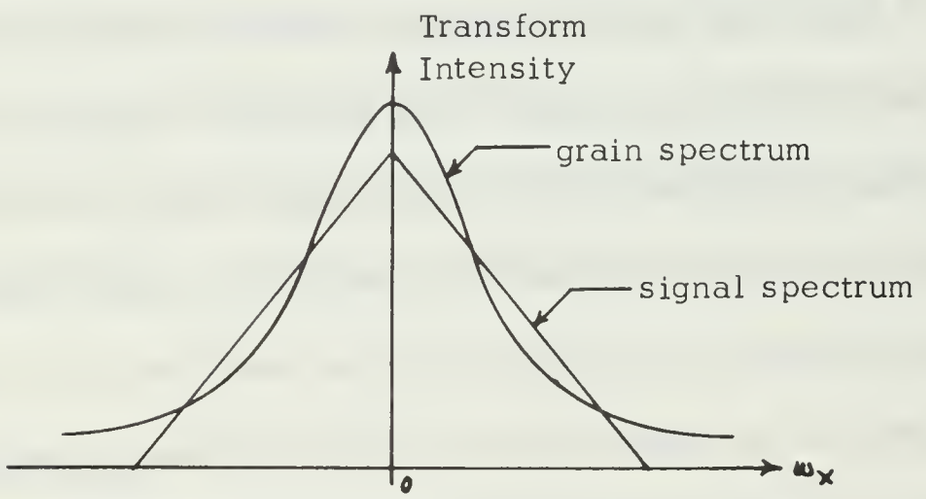

Figure 21. Idealized signal and grain spectrums for a signal on coarse grain film.

some high frequency limit, the signal spectrum intensity will be less than the grain spectrum intensity. Under these conditions, the grain structure is seen to have a greater effect on the high frequencies or the fine detail of the signal. Figure 21 illustrates a case similar to that of Figure 20, but one in which the grains are coarse. This case resembles the experimental results. In Figure 21, the grain spectrum intensity is greater than the signal spectrum intensity at both low and high frequencies and effectively creates a pass-band. The high frequency limit was not observed in Figures 18 and 19 because the intensity range in the output exceeded the film density recording range. Further, since the grain transform intensity obscured most of the important lower signal frequencies in Figures 18 and 19, reconstruction of the signal by Fourier transform of the output transparency was found to be impossible.

Thus, film grain in a coherent optical system has an effect similar to noise in electrical circuits. The film grain spectrum in the limiting case of Figure 20 appears similar to Gaussian noise in that its spectrum is flat over the range of interest. It appears that in many cases involving binary signals on fine grain film, this noise could be assumed Gaussian, at least as an approximation. In the discussion relating to Figures 15 and 16, it was noted that the film grain spectrum is a function of the film density for densities other than D_{min} and D_{max}. This would mean that there would necessarily be some correlation between grain noise and a signal comprising intermediate densities. The assumption of Gaussian noise could then be, at best, an approximation.

III. DETECTION OF SHIPS BY KELVIN WAVE

A. INTRODUCTION

The wave pattern produced by a pressure disturbance moving on the surface of the water was first considered by Lord Kelvin [15] in 1891. For a disturbance such as a ship moving on a straight course, the wave height is considerable inside an angle bounded by two horizontal rays at ±19.5 degrees with respect to the ship's course line [16]. Further, the angle is not a function of speed. Such a pattern, when considered against a random sea wave pattern, is unique and optical Fourier transforming techniques may be applied for its detection.

The method used in this project was the single transform of a wake photograph with a matched filter in the first transform plane. The matched filter was rotated on the optical axis and the resulting transmitted light measured with a CdS cell to examine the possibility of further electrical filtering. A thorough investigation was not conducted since this was considered as a feasibility study and as a practical use-test of the optical system.

B. THE WAVE PATTERN

The free surface equation of ship waves is very difficult to derive when exact hydrodynamical theory is used. The solution of Lord Kelvin's as well as later work are approximations [16 and 17]. Even then the results are quite involved and not completely germane to the problem of

detecting the waves. Ursell [16] has predicted and plotted contours for a ship's wave near the critical angle, θ=19.5 degrees. Figure 22 is one of these plots.

Along the critical angle, the wave crests are inclined at an angle of 54.75 degrees to the track of the ship. Outside the critical angle, the wave height falls rapidly to zero. The horizontal angle of inclination between wave crests and the track decreases from 54.75 degrees to zero degrees for angles from less than θ_c to points on the track. However, the wave height also decreases inside θ_c although not as rapidly as outside θ_c. Thus there is some horizontal inclination angle between 54.75 degrees and zero degrees at which the wave heights become insignificant. By way of comparison, the wave heights near the critical angle die out as an inverse function of the cube root of distance while, in the interior, they die out as an inverse function of the square root of distance [18]. The wave height and period are functions of the ship's speed and, from Figure 22, it can be seen that the period also decreases with angle. In summary, as the angle decreases from θ_c to zero, the wave height decreases, the wave period decreases, and the wave crests' angle of inclination with respect to the track decreases (normal angle increases). These factors allow a qualitative prediction of the Fourier transform of such a pattern to be of the form in Figure 23. θ_A is the direction of wave travel (normal angle) for wave components near θ_c, and θ_B is the direction of wave travel for wave components which exist near the track. θ_A equals 90-54.75 degrees or 35.25 degrees.

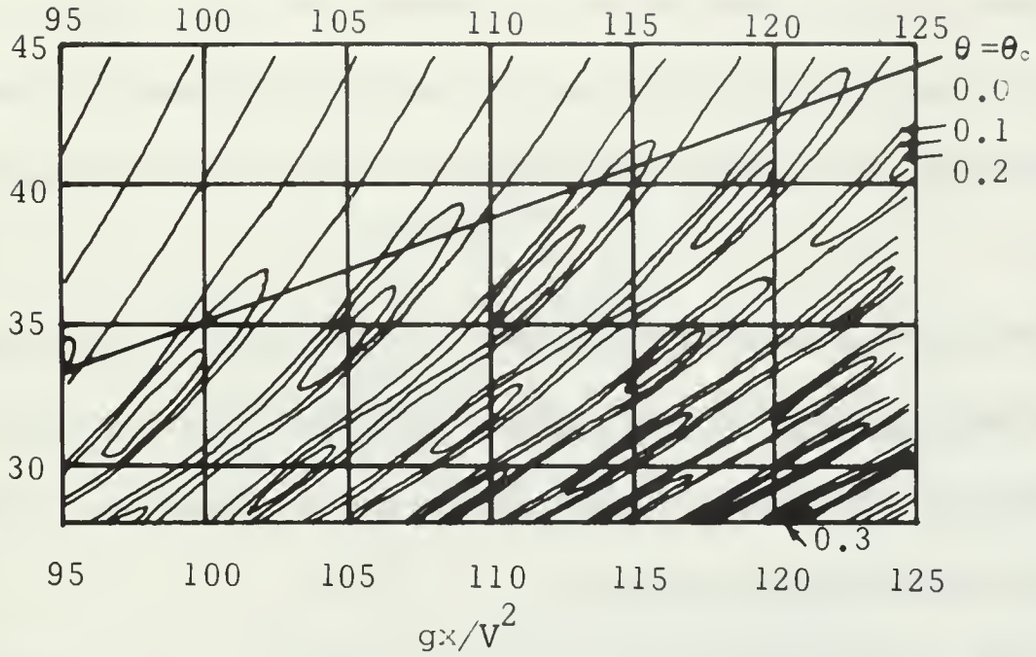

Figure 22. Contours of equal magnitude of the dimensionless surface elevation $\rho V^2 \zeta_2(x,y)/2gP_o$ due to a concentrated force P_o moving with velocity V, for $gr/V^2 = 2\pi r/\lambda$ near 100. (Here r denotes the distance from the disturbance, λ the wavelength of waves moving with phase velocity V.) For the sake of clarity only positive values of the elevation are shown. [After Ursell, Ref. 16].

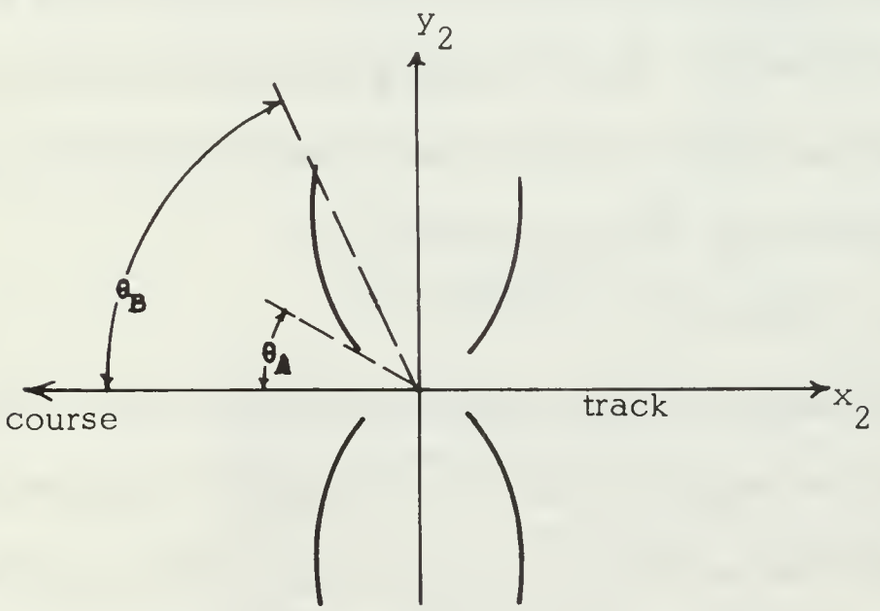

Figure 23. Approximate Fourier transform of a ship's wave.

C. PHOTOGRAPHIC PROPERTIES

Stillwell [19] analyzed the relation between the light scattered from a sea surface and the optical density of a scene photograph. The method is outlined here with some changes which are necessary to the present problem.

Let the ship's wave height pattern be described by $H(x,y)$, where x and y are taken to be on the sea surface. Assume the sea surface is illuminated by a completely clear or a completely overcast sky. The illumination at the camera becomes:

$$M(\eta) = KN(\mu)\Gamma(\beta_o) \qquad (3\text{-}1)$$

where K is a constant, $L(\theta)$ the luminance of the sky in the direction reflected into the camera, and $\Gamma(\beta_o)$ is the reflectivity at the incident angle β_o. Figure 24 describes the geometry for a one-dimensional surface. For the two-dimensional surface, β_o and θ are simple functions of δ and σ. The water reflectivity is a function of the incident angle and this is illustrated in Figure 25. Thus the camera illumination under these conditions is a function of the sea surface wave height structure, $H(x,y)$. The camera illumination can now be described as:

$$M(x,y) = K_1 H(x,y) \qquad (3\text{-}2)$$

where K_1 is a constant. (Note: The illumination is also a function of the angle over the field covered by the photograph. The illumination is maximum directly away from the observer and is present in all sea photographs [19]. A narrow field of view will be assumed so that this factor is eliminated.) Using equation (2-12), the recorded film density is:

$$D(x_1,y_1) = \gamma \log I(x_1,y_1)T + K_2(\text{constant}) \qquad (3\text{-}3)$$

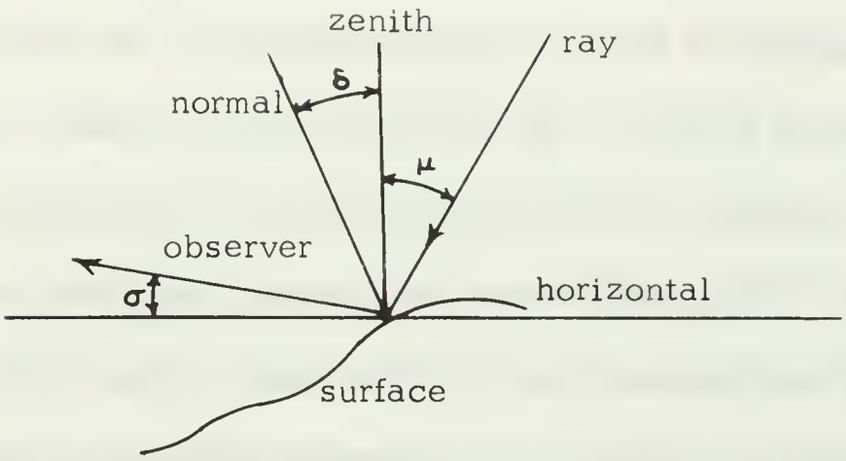

Figure 24. One-dimensional sea surface reflection geometry.

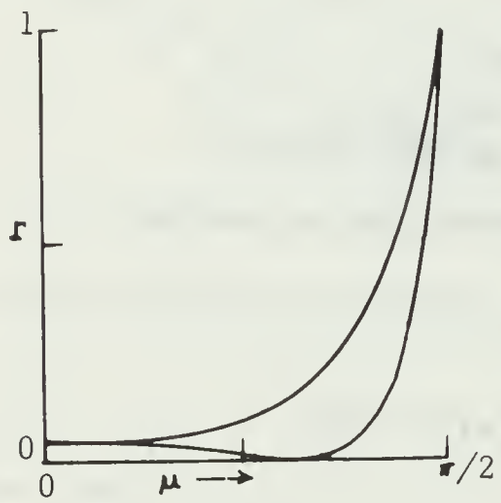

Figure 25. Water reflectivity. In the visible region, water reflectivity is related to the angle from the normal by the above curve. In addition to the wavelength dependence of the reflectivity, the vertically (V) and horizontally (H) polarized components have different reflectivities. [After Stillwell, Ref. 19].

where T is the exposure time and the coordinates, (x_1, y_1), are in the film plane. Figure 26 illustrates the relation between the surface coordinates, (x,y), and the film coordinates, (x_1, y_1). The magnification, m, is a function of the film to object distance. Assuming $r_1'+r_2'$ is approximately equal to r_1+r_2 over the region recorded, then m may be assumed constant over the region and simple trigonometric relations may be applied. This approximation is generally true since the camera height is usually much greater than the focal length. The coordinates, x and x_1, are arbitrarily assumed to be in horizontal planes such that the relation, $x_1=mx$, holds. The coordinates, y and y_1 are then in a vertical plane containing both y and y_1. The plane, P', is drawn normal to the line of sight and the coordinates related to this line become:

$$x_1 = mx'$$

$$y_1 = my'$$

$$\text{and } 0 < m < 1 \qquad (3\text{-}4)$$

The following angles may be derived.

$$\theta = 90 - \sigma$$

$$\epsilon = \sigma - \sin^{-1} \frac{y_1/m}{r} \qquad \text{for } r >> r_1$$

$$\nu = 90 + \sin^{-1} \frac{y_1/m}{r}$$

And finally, the Law of Sines,

$$\frac{y_1/m}{\sin \epsilon} = \frac{y}{\sin \nu} \qquad (3\text{-}5)$$

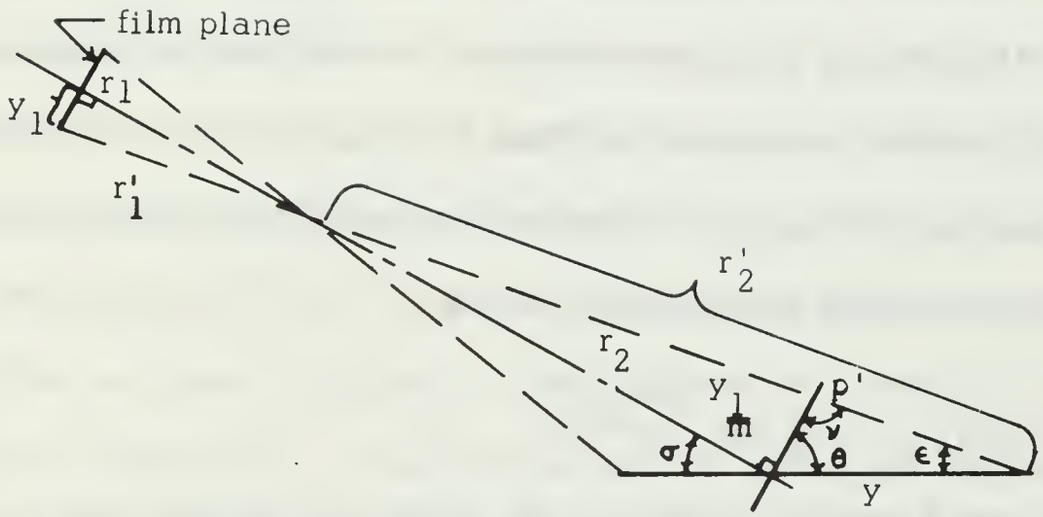

Figure 26. Sea surface-film plane geometry.

gives the required relation.

$$y_1 \simeq \frac{my \sin \sigma}{1 + y/r} \tag{3-6}$$

For a high altitude camera such as in a satellite, σ is approximately 90 degrees and equation (3-5) becomes,

$$y_1 = my$$

and (3-7)

$$x_1 = mx$$

D. THE SHIP WAVE TRANSFORM

The exposed photograph contains the sea surface information in the form of density variations as given by equation (3-3). This transparency is inserted into the input plane of a single Fourier transform system. The transmitted light amplitude is given by:

$$f_1(x_1, y_1) = f_o \, 10^{-\frac{D(x_1, y_1)}{2}} \tag{3-8}$$

The light intensity function in the output or transform plane is:

$$I_p(x_2, y_2) = k_3 \left| \mathcal{F}[f_1(x_1, y_1)] \right|^2 \tag{3-9}$$

Combining equations (3-2, 3, 8, and 9), the final expression is:

$$I_p(x_2, y_2) = K_4 \left| \mathcal{F}[H(x,y)^{-\gamma/2}] \right|^2 \tag{3-10}$$

where: $K_4 = K_3(f_o \, 10^{K_2 K_1 T})^2$ and x, y are given by equation (3-6) or (3-7)

Although the above method is not complete and includes several assumptions, the results are sufficient to verify the existence of a predictable relationship between a ship wave and the Fourier transform of its photograph.

In a practical situation the ship wave must be considered in the presence of sea waves. The sea waves will not have the unique Fourier transform of the ship wave and, on the basis of this alone, should be easily separated in the transform plane. However, the sea waves do contribute to an overall noise level and it may be assumed that there is some minimum ratio of ship wave height to sea wave height below which the optical detection would be useless. Later mention will be made of this in section IV.

E. A SHIP WAVE DETECTION EXPERIMENT

The photograph of Figure 28 is a ship wave in a low sea state. The characteristic features are readily apparent along the critical angle. The transparency for Figure 28 was inserted in the input plane of the optical system illustrated in Figure 27, and an exposure was made in the transform plane. This is shown in Figure 29. The transform was similar to that predicted in section III-B. The differing density of the two pairs of wave lines may be traced to Figure 28 where the location of the sun produced differing modulation levels on the two sides of the wake. It was noted that this affected primarily the density rather than the shape of the output transform. The remainder of the pattern is composed of the grain transform and the central DC intensity considered in section II, and the transform of the sea waves which appear as noted in Ref. 19.

A crude matched filter was produced by cutting out the portion of Figure 29 which represents the ship wave alone. This filter was then aligned in a mount which allowed rotation of the filter about a plane

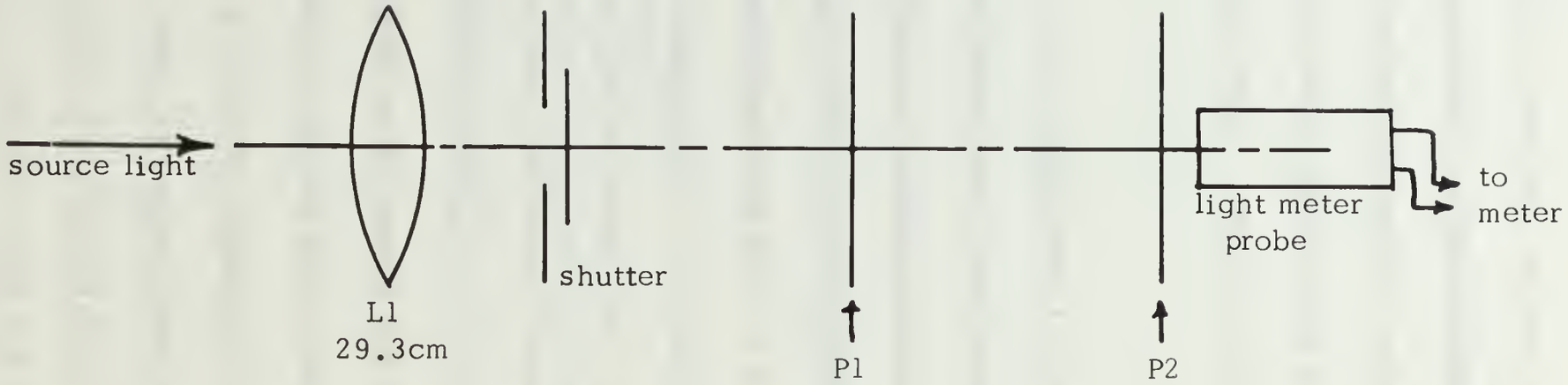

Figure 27. Optical system diagram for the ship wave transform.

Figure 28. Ship wave in a low sea state.

Figure 29. Fourier transform of the ship wave of Figure 28.

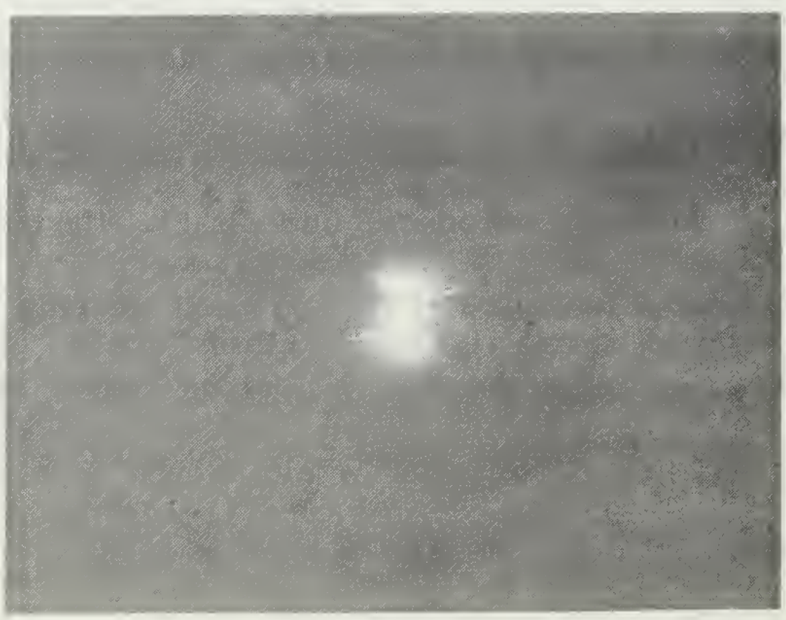

normal to the optical axis. The mounted filter was placed at plane, P2, and a CdS cell covered with diffusing glass placed behind it. The geometry was designed so that the area of the transform pattern matched the CdS cell face. The cell output was then read as a function of angular filter position.

This particular experimental arrangement was chosen to investigate the possibility of performing additional filtering by rotation of the matched filter at a constant rate. The CdS cell output would then be a time correlation of the signal and the matched filter. However, it must be noted that a CdS cell has a slow response time and could not be used at practical rotation speeds. Referring to Figure 29, the output should consist of an average level plus components due to sea waves and the ship wave with a fundamental frequency of twice the rotation rate. The ship wave component would have a shorter time duration and produce different frequency harmonic terms. The resulting data is presented in Figure 30. This is the best run of a series. The data not included here was similar to that of Figure 30 but, in general, was degraded by inaccurate filter construction and filter centering. The construction problem could have been eased by using a photographic transparency filter, however, this would also have introduced undesirable film grain effects. The portion of the curve in Figure 30 representing the ship wave is quite prominent and suggests the possibility of visual detection. However, since the intended use of the output would involve frequency analysis, the curve was analyzed further for frequency content.

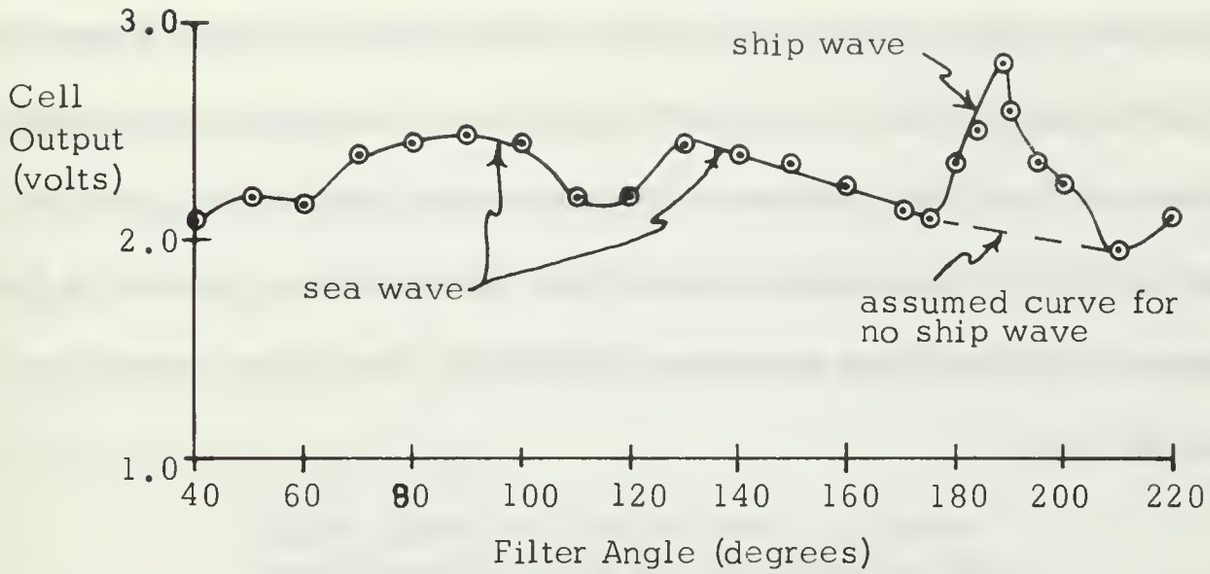

Figure 30. Ship wave detection output voltage curve. Each point is the average of V_θ and $V_{\theta+180}$ to minimize the effects of misalignment.

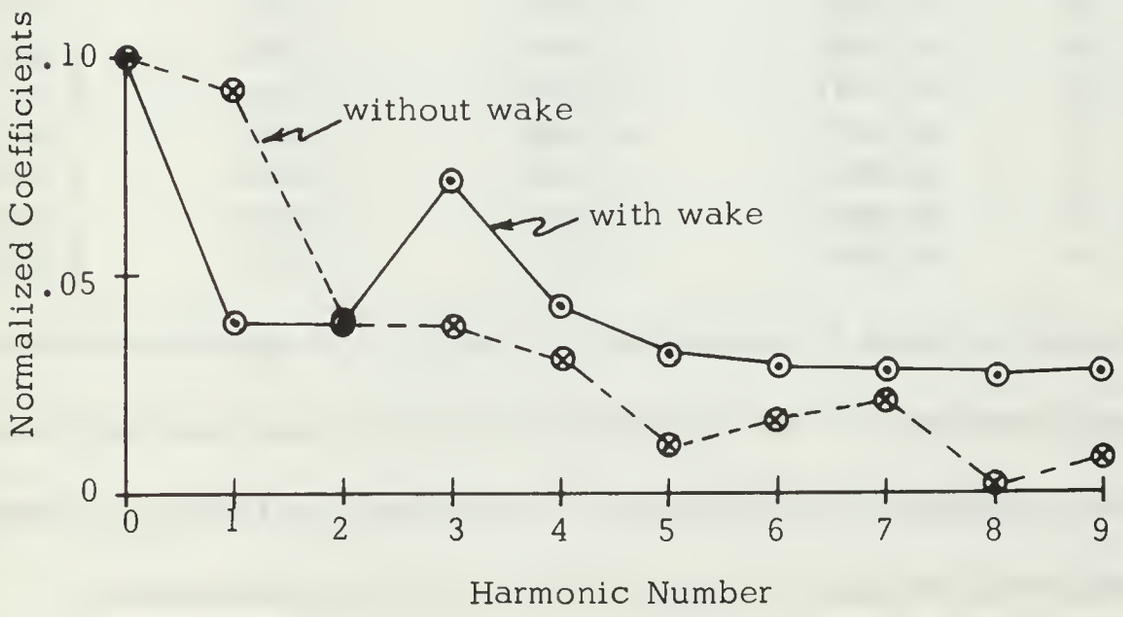

Figure 31. Ship wave detection. Fourier series coefficients of output electrical signal. (Curve joining points is only for clarity.)

The FORTRAN program, FORIT, which computes Fourier series coefficients for a tabulated, periodic function was used for frequency analysis. Nineteen equally spaced points over 180 degrees of Figure 30 were used to obtain coefficients to the ninth harmonic. For comparison a similar curve, in which the ship wave component was replaced by a straight line joining the component end-points. The resulting exponential Fourier series coefficients are presented in Table II. The values normalized to the DC level

TABLE II. EXPONENTIAL FOURIER SERIES COEFFICIENTS OF THE CdS CELL OUTPUT.

HARMONIC	COEFF. WITH WAKE	COEFF. W/O WAKE	NORMALIZED WITH WAKE	NORMALIZED W/O WAKE
0	2.3341v	2.2552v	1.0000	1.0000
1	0.0927	0.2084	0.0397	0.0927
2	0.0871	0.0883	0.0373	0.0397
3	0.1665	0.0881	0.0713	0.0392
4	0.0995	0.0690	0.0426	0.0307
5	0.0726	0.0263	0.0311	0.0117
6	0.0679	0.0392	0.0291	0.0174
7	0.0642	0.0486	0.0275	0.0216
8	0.0490	0.0038	0.0210	0.0017
9	0.0543	0.0179	0.0233	0.0080

are given in Table II and plotted in Figure 31. A marked difference was noted particularly in the fundamental and the second and third harmonics. It was concluded that the output is susceptable to frequency filtering to indicate the presence of a ship wave in the input transparency.

F. CONCLUSIONS

Thus, the combined optical-electrical detection of a ship wave has been shown to be feasible, at least on a crude level. Since the transform of a ship's wake is always centered on the optical axis, the system is

not dependent on the wave position in the input field. The rotation of the matched filter eliminates the dependence on angular positioning. A phase reference derived from the filter rotation drive could conceivably be used to determine the ship's course with a 180 degree ambiguity by comparison of the phase of the ship wave component in the output signal to the phase reference. These factors suggest the use of such a system in an automatic alarm system to indicate the presence of a moving vessel in some monitored area of the ocean.

IV. SUGGESTIONS FOR FURTHER RESEARCH

A. FILM CHARACTERISTICS

The film grain model developed in section II allowed a semi-quantitative prediction of the grain transform. The ultimate limitation of this method lies in the grain model itself. However, the results would have been more useful with a closed mathematical expression for the total transform with the input size-frequency distribution known. As stated before, from equation (2-7), this involves the distribution function of the output which is obtained by finding the inverse of the term $2J_1(Z)/Z$. The expression for the grain transform could be obtained in a closed form if this stumbling block were overcome. Since the input size-frequency distribution is often known for a type of film, the results could be applied almost directly to predict the effects of grain for any film type.

B. SHIP WAVES

The ship wave detection problem has been treated here on a fairly basic level with several approximations and assumptions. Since the concept does have obvious applications in surveillance of the seas, it seems worthwhile to define the problem more fully. Some of the problems involved are: (1) the variation of reflected light modulation with the sun and observer positions, (2) the relation between a ship wave and sea waves travelling at various relative surface angles, and (3) the signal to noise ratio.

C. SEA SURFACE ENERGY SPECTRA

In Ref. 19, Stillwell describes the use of a single optical Fourier transform system to determine the energy spectrum of sea surface wave heights or wave slopes. Research into this area is of importance not only to oceanographers but is also vital to studies in radar scattering and acoustic propagation.

A brief outline of Ref. 19 is given here. As noted in section III, the light arriving at a camera above a sea surface is a function of the wave slopes because of the incidence angle dependence of water reflectivity. The density of the exposed film is then determined by the sea surface characteristics and the problem geometry. The optical Fourier transform of such an exposed film can be expressed in terms of the film density and source light intensity. Since the transform output records the spatial frequency components of the input, it will also represent the sea surface spatial frequency components with a scale or magnitude factor involved. It is shown that the spatial frequency components of the sea surface are related to the slope energy spectrum, which is expressed as:

$$\Phi(K_1\psi) = C\ 10^{\frac{D(k/m,\psi)}{\gamma}} \sec^3\psi \qquad (4\text{-}1)$$

where C is a constant, $D(k/m,\psi)$ is the output or transform photograph density function, k is the radian wave number, m is the magnification factor, ψ is an angle between the observer-surface normal plane and the observer-zenith plane. $\psi = 0$ on a line directly away from the observer. Stillwell presents some results by plotting density contours of the transform output. A typical contour is shown in Figure 32.

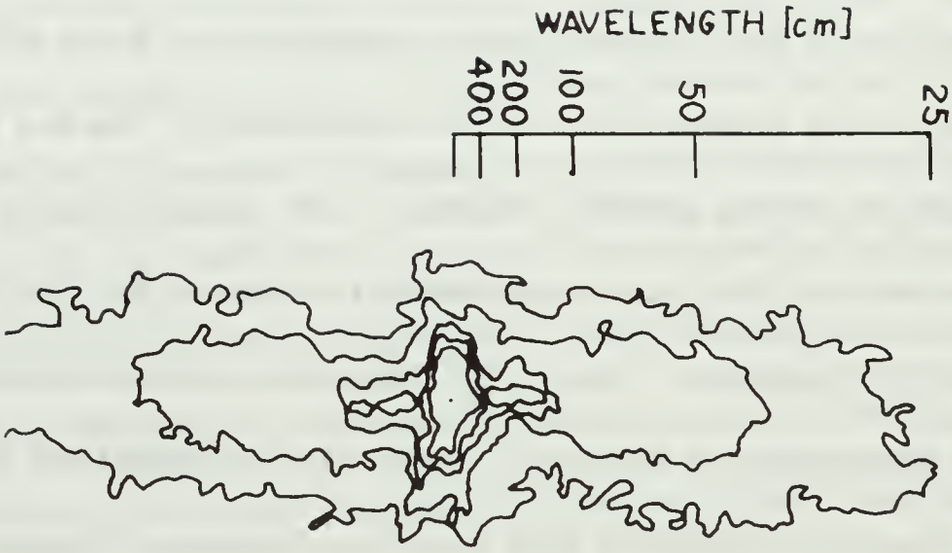

Figure 32. Density contours showing the long wavelength spectrum and spectral peak for a light to moderate wind of long fetch. [After Stillwell, Ref. 19].

Several attempts at analyzing sea surface photographs were made using the present optical system. The original photographs were 8X10 inch transparencies, of which an area of $4\frac{1}{2}X4\frac{1}{2}$ inches was selected and reduced to 1/20th size. The area selected is shown in Figure 33 and the transform output in Figure 34. A microdensitometer was used to obtain the contours in Figure 35. The results were generally unsuccessful but not totally so. The contours do indicate some pattern which could only be attributed to the sea surface structure, and they are roughly similar to those in Figure 32. Most of the difficulties can be traced to the quality of the input. The original 8X10 inch transparency was grainy and the reduction of a photograph usually entails some loss of high frequency content. Both of these factors are apparent in Figures 34 and 35, and they are serious enough to make the reduced negative virtually useless.

It is suggested that further work might be done in this area using sea surface photographs taken for the prime purpose of use as inputs to the optical Fourier transform system.

Figure 33. Sea surface photograph.

Figure 34. Fourier transform of sea surface of Figure 33.

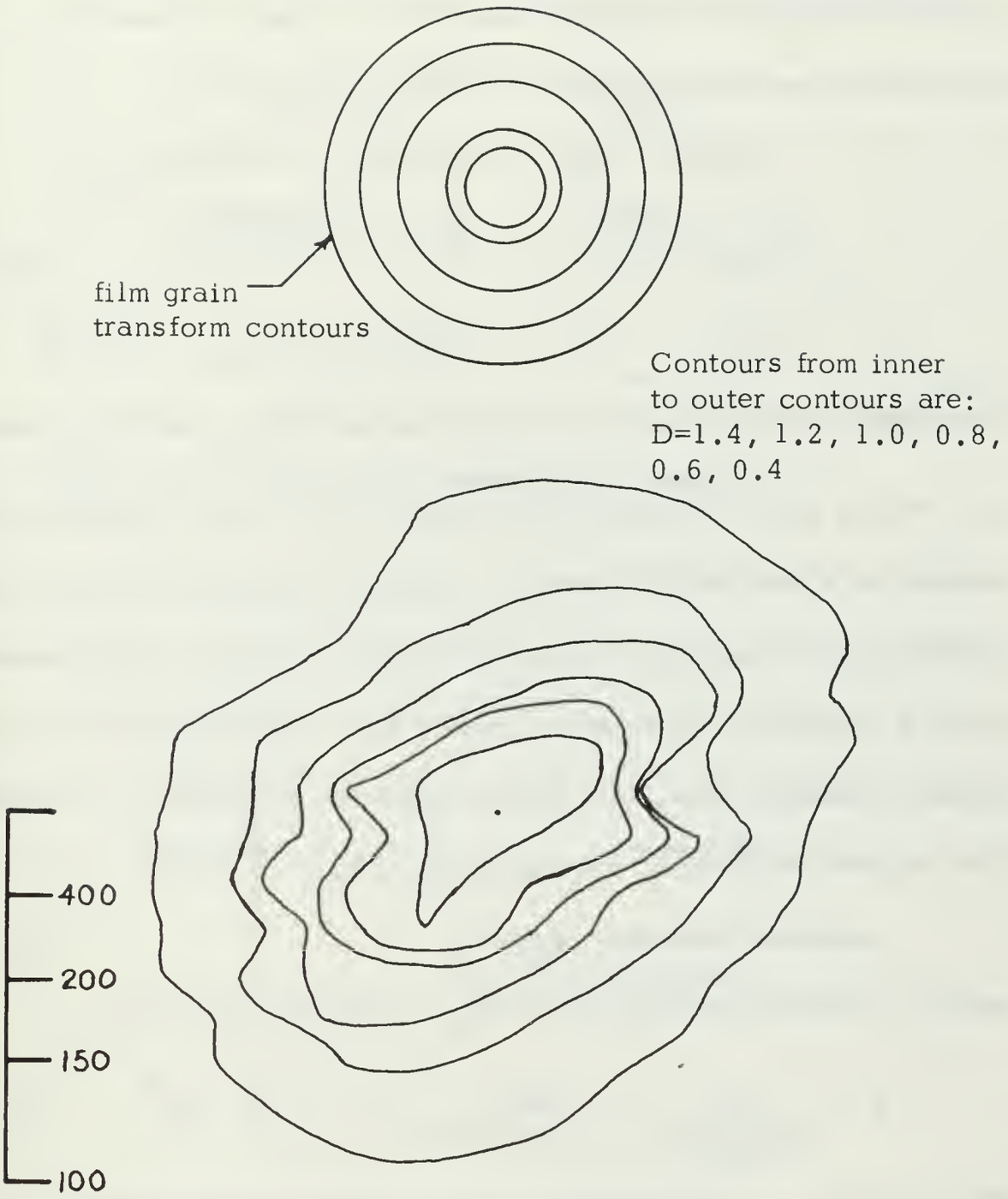

Figure 35. Density contours of Figure 34.

APPENDIX A. FILM CHARACTERISTICS

The typical D/logE curve has the form of Figure 36. A standard approximation for the negative type film is shown in Figure 37. The resulting equation which describes the curve of Figure 37 is:

$$D = \begin{cases} \gamma[\log E - \log i] & \text{for } E(D_{min}) < E < E(D_{max}) \\ D_{max} & \text{for } E \geq E(D_{max}) \\ D_{min} & \text{for } E \leq E(D_{min}) \end{cases} \qquad \text{(A-1)}$$

Often the spectral sensitivity curve, gamma, D_{max}, and D_{min} are the only values given. Equation (A-1) must then be used to determine the density as a function of exposure. Spectral sensitivity curves relate radiant light intensity (or energy density) as a function of wavelength to reach a specified film density, usually 0.5. The exposure, E, is the incident luminous flux, U, times the duration of exposure. Luminous flux and radiant flux, R, are related by [20]:

$$\text{luminous efficiency } (\eta) = \frac{U}{R} \qquad \text{(A-2)}$$

which is 150 lumens/watt for 6328Å. The exposure is then:

$$E = \frac{UT}{\text{unit area}} = \frac{\eta RT}{\text{unit area}} \qquad \text{(A-3)}$$

The constant, i, is evaluated using the radiant light intensity for D=0.5 from the spectral response curve. The result is:

$$D = \gamma\,[\log E - \log E(D=0.5)] + 0.5 \qquad \text{(A-4)}$$

$$\text{for} \quad E(D_{min}) < E < E(D_{max})$$

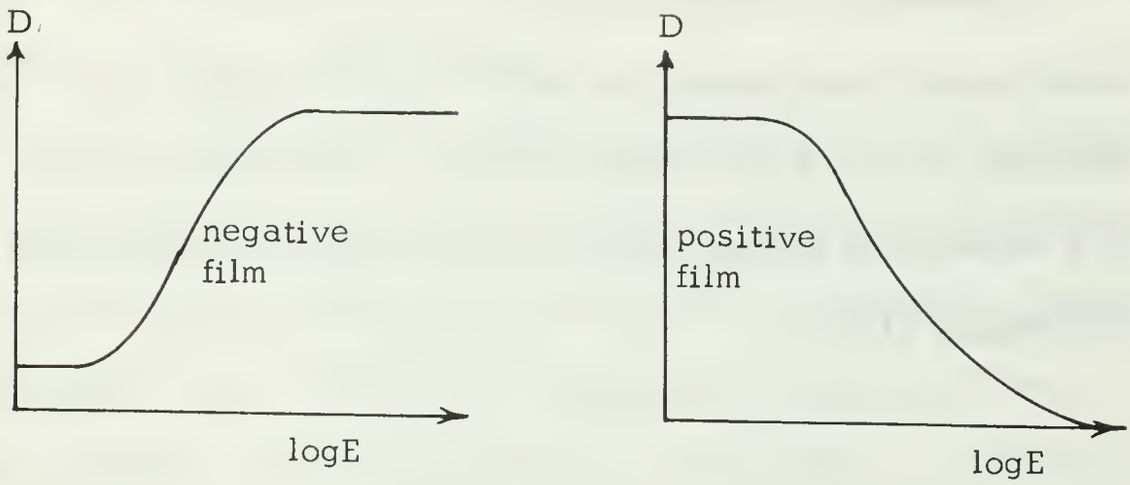

Figure 36. Typical film characteristic curves.

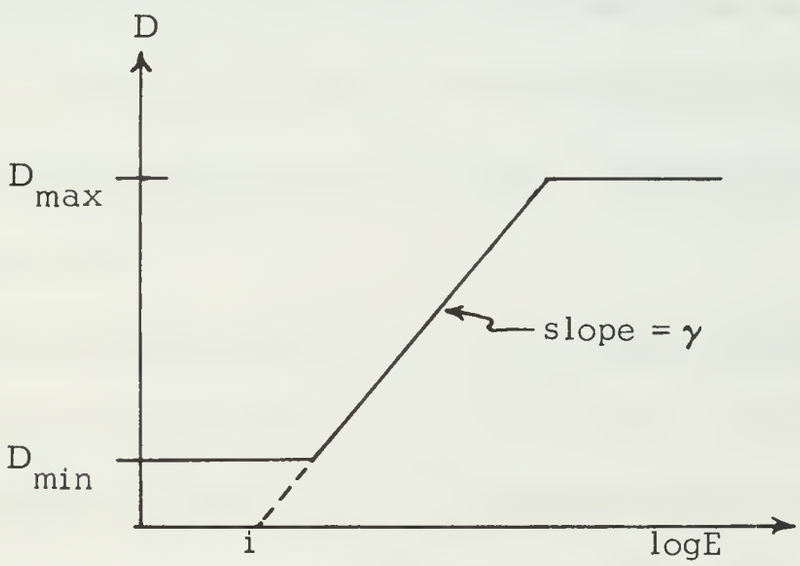

Figure 37. Approximation of the film characteristic curve.

When exact light levels are not known or desired, the following form is useful.

$$D = \gamma \log E + \text{constant} \qquad \text{(A-5)}$$

The effect of reciprocity failure is not considered here. Reciprocity failure occurs when exposures involve a high intensity and a very short exposure time or a low intensity and very long exposure time. The effect is a reduction of film sensitivity and the exposure time must be increased accordingly [11].

APPENDIX B. LIGHT INTENSITY METER

The light intensity meter described here was found useful in conjunction with the optical system. It can provide a rough measure of the intensity distribution at any point in the system and eliminate some of the guess work to obtain a proper exposure.

The circuit is diagrammed in Figure 38 and is basically a high gain operational amplifier with a cadmium sulfide photocell in the feedback loop [23]. This configuration was used to reduce the effects of temperature and power supply variations. Transistors Q_1 and Q_2 act as a differential amplifier with a 1.5 volt input. Transistor Q_3 is a DC level shifter and amplifier while transistor Q_4 drives the meter.

The photocell was mounted in a telescopic tube behind a 0.5mm diameter pinhole. The telescopic tube was affixed to a bracket with vertical and horizontal tracks so that the photocell position could be adjusted over the face of the bracket. The bracket slides into the film pack holder with the pinhole in the film plane. The completed unit is shown in Figure 39.

The unit was calibrated from zero to 2990 meter-candles using diffuse illumination and a Weston Illumination Meter. There was no standard available to calibrate the meter above 2990 meter-candles. The calibration above 2990 meter-candles was accomplished by comparing the readings at two distances from the source. Letting $I_c(d)$ define a calibrated reading at distance d, the relation is:

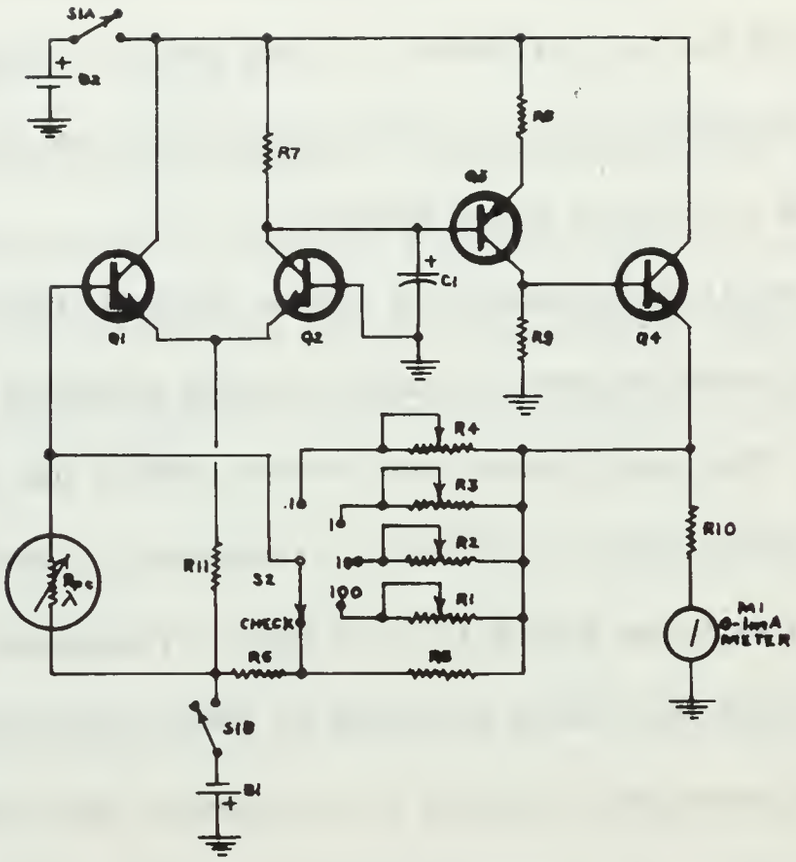

R1-500 ohm pot
R2-2500 ohm pot
R3-25,000 ohm pot
R4-100,000 ohm pot
R5-10,000 ohm, $\frac{1}{4}$W
R6-3000 ohm, $\frac{1}{4}$W
R7-1000 ohm, $\frac{1}{4}$W
R8, R11- 470 ohm, $\frac{1}{4}$ W
R9-10,000 ohm, $\frac{1}{4}$ W
R10-2700 ohm, $\frac{1}{4}$ W
R_{pc}-Clairex CL505-L

C1-10uf, 15V elec.
S1-DPST, normally open
S2-SP, 5 pos. selector switch
B1-1.5V
B2-9V
Q1, Q2-2N3391
Q3-2N4126
Q4-2N3391

Figure 38. Light Intensity Meter circuit. [After Barnum, Ref. 21].

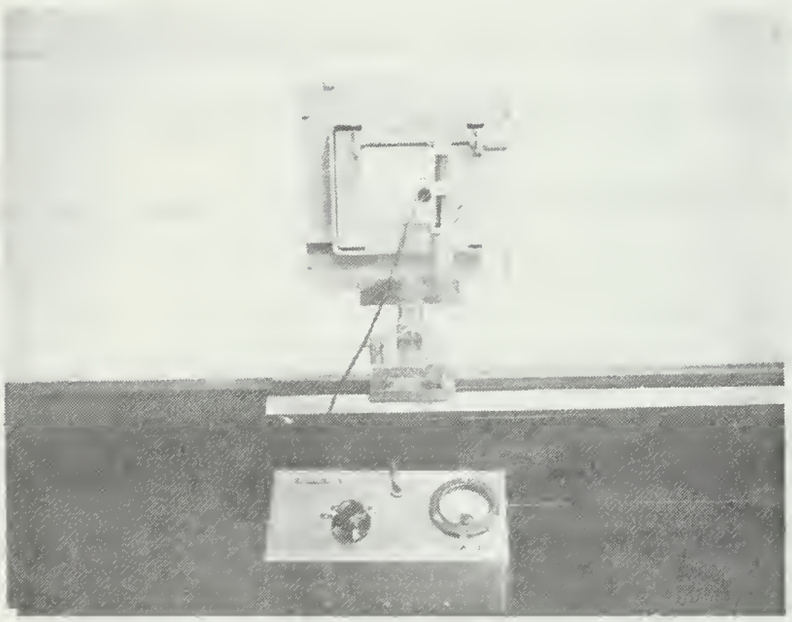

Figure 39. Light Intensity Meter

$$\frac{I_c(d_1)}{I_c(d_2)} = \text{constant, } K \qquad \text{(B-1)}$$

The distances, d_1 and d_2, were used for all readings and the readings outside the calibrated range become:

$$I_{\text{uncalibrated}}(d_1) = KI_c(d_2) \qquad \text{(B-2)}$$

The resulting accuracy cannot be as close as ±5%. The calibration curves are given in Figure 40. A fourth meter scale was not calibrated because a light source of such high intensity was not available. This scale is beyond the range of intensities in the optical transform system and was not needed.

In use, the probe is positioned to monitor the light intensity in a region of the output plane where a linear density response is desired. An approximately correct first exposure can be obtained by exposing for a density of 1.0 for most films [11]. Equation (A-4), solved for E to reach a density of 1.0, becomes:

$$E = E(D=0.5)\ 10^{0.5/\gamma} \qquad \text{(B-3)}$$

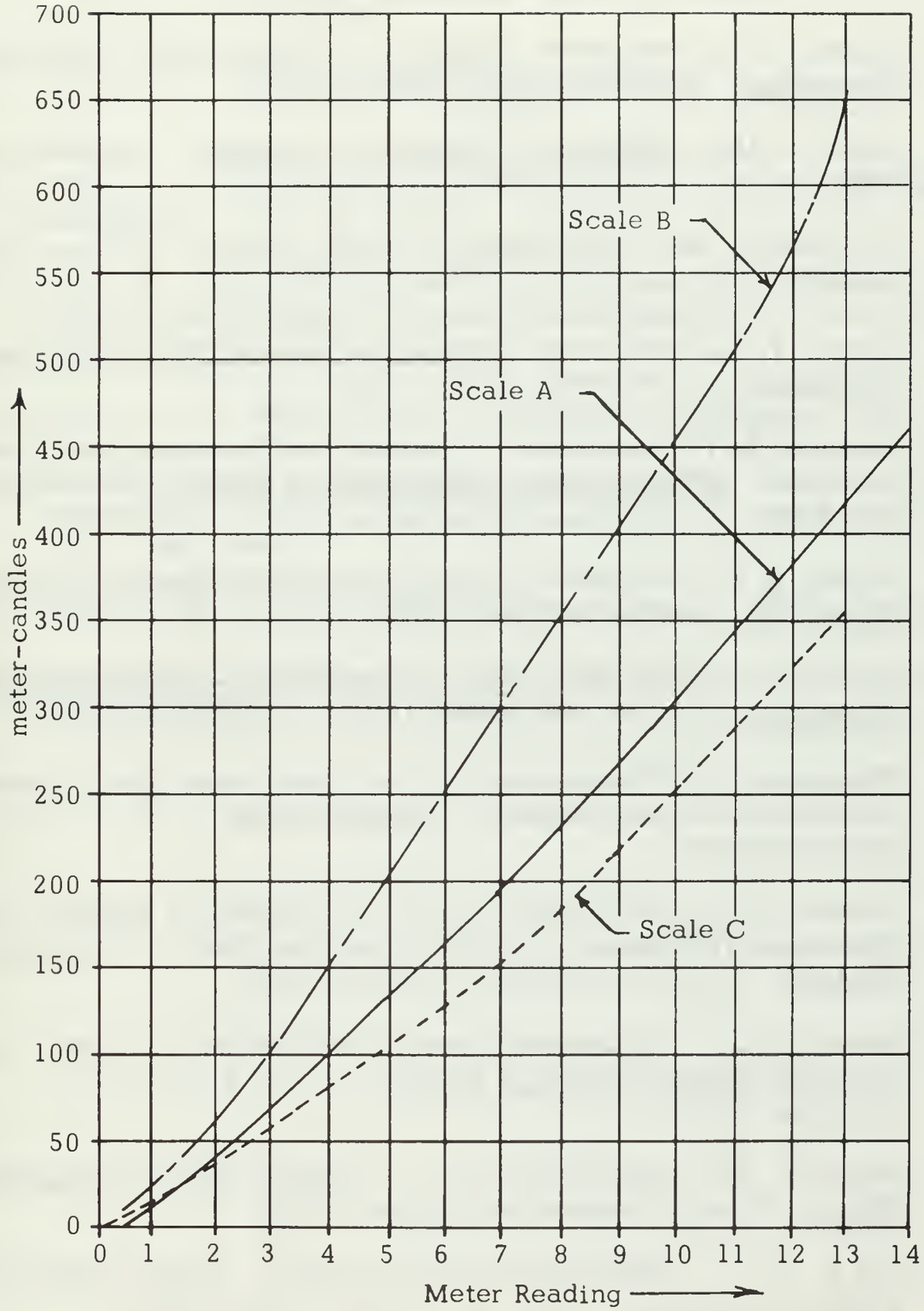

Figure 40. Light Intensity Meter calibration curves. Scale readings are: X1 for Scale A(±5%), X10 for Scale B(± 5% for meter reading less than 7 and 10% above 7), and X100 for Scale C (±20%). Functional tests: BATTERY-13.3 meter reading; CHECK-9.2 meter reading.

BIBLIOGRAPHY

1. Tippet, J. T., and others, Optical and Electro-Optical Information Processing, p. 59-68, MIT, 1965.

2. Francon, M., Diffraction, Coherence in Optics, Pergamon Press, 1966.

3. Goodman, J. W., Introduction to Fourier Optics, McGraw-Hill, 1968.

4. Tippet, J. T., and others, Optical and Electro-Optical Information Processing, p. 143-158, MIT, 1965.

5. Cutrona, L. J., and others, "Optical Data Processing and Filtering Systems," IRE Transactions or Information Theory, p. 386-400, June 1960.

6. Tippet, J. T., and others, Optical and Electro-Optical Information Processing, p. 83-122, MIT, 1965.

7. Tippet, J. T., and others, Optical and Electro-Optical Information Processing, p. 125-141, MIT, 1965.

8. Upatnieks, J., "Improvement of Two-Dimensional Image Quality in Coherent Optical Systems," Applied Optics, v. 6, p.1905-1910, November 1967.

9. Cutrona, L. J., and others, "On the Application of Coherent Optical Processing Techniques to Synthetic-Aperture Radar," Proceedings of the IEEE, v. 54, p.1026-1032, August 1966.

10. Jones, R. C., "Information Capacity of Photographic Films," Journal of the Optical Society of America, v. 51, p.1159-1171, November 1961.

11. James, T. H., and Higgins, G. C., Fundamentals of Photographic Theory, 2d ed., Morgan and Morgan, 1960.

12. Yu, F. T. S., "Markov Photographic Noise," Journal of the Optical Society of America, v. 59, p. 342-344, March 1969.

13. Montgomery, W. D., and Broome, P. W., "Spatial Filtering," Journal of the Optical Society of America, v. 52, p. 1259-1275, November 1962.

14. Goodman, J. W., "Film-Grain Noise in Wavefront-Reconstruction Imaging," Journal of the Optical Society of America, v. 57, p. 493-502, April 1967.

15. Lord Kelvin, Proceedings of the Royal Society, v. 42, p. 80, 1887.

16. Ursell, F., "On Kelvin's Ship-Wave Pattern," Journal of Fluid Mechanics, v. 8, p. 418-431, July 1960.

17. Peters, A. S., "A New Treatment of the Ship Wave Problem," Communication of Pure and Applied Mathematics, v. 2, p. 123-148, 1949.

18. Stoker, J. J., Water Waves, Interscience Publishers, 1957.

19. Stillwell, Jr., D., "Directional Energy Spectra of the Sea from Photographs," Journal of Geophysical Research, v. 74, p. 1974-1986, April 1969.

20. Sears, F. W., Optics, Addison-Wesley Press, 3d ed., 1949.

21. Barnum, J. L., "Design of a Light Meter and Exposure Calculator," Electronics World, v. 81, May 1969.

INITIAL DISTRIBUTION LIST

		No. Copies
1.	Defense Documentation Center Cameron Station Alexandria, Virginia 22314	20
2.	Library, Code 0212 Naval Postgraduate School Monterey, California 93940	2
3.	Naval Air Systems Command Headquarters Washington, D. C. 20350 Attn: AIR-370D	1
4.	Asst. Professor G. L. Sackman, Code 52Sa Department of Electrical Engineering Naval Postgraduate School Monterey, California 93940	5
5.	Professor S. H. Kalmbach, Code 61Kb Department of Physics Naval Postgraduate School Monterey, California 93940	1
6.	Professor W. P. Cunningham, Code 61Cm Department of Physics Naval Postgraduate School Monterey, California 93940	1
7.	LT Robert Dale Ferguson, USN 1005 Halsey Drive Monterey, California 93940	1
8.	Professor T. Green Department of Meteorology University of Wisconsin Madison, Wisconsin 53706	1
9.	D. H. Brown, Code 722 United States Navy Ship Research and Development Laboratory Panama City, Florida	1

Security Classification

DOCUMENT CONTROL DATA - R & D

(Security classification of title, body of abstract and indexing annotation must be entered when the overall report is classified)

1. ORIGINATING ACTIVITY (Corporate author)	2a. REPORT SECURITY CLASSIFICATION
Naval Postgraduate School Monterey, California 93940	Unclassified
	2b. GROUP

3. REPORT TITLE

An Experimental Single Fourier Transform Optical Processor
Applied to Film Grain Analysis and A Ship Wave Detection Method

4. DESCRIPTIVE NOTES (Type of report and inclusive dates)

Electrical Engineer and Master of Science in Electrical Engineering; December 1969

5. AUTHOR(S) (First name, middle initial, last name)

Robert Dale Ferguson

6. REPORT DATE	7a. TOTAL NO. OF PAGES	7b. NO. OF REFS
December 1969	83	21

8a. CONTRACT OR GRANT NO.	9a. ORIGINATOR'S REPORT NUMBER(S)
b. PROJECT NO.	
c.	9b. OTHER REPORT NO(S) (Any other numbers that may be assigned this report)
d.	

10. DISTRIBUTION STATEMENT

This document has been approved for public release and sale;
its distribution is unlimited.

11. SUPPLEMENTARY NOTES	12. SPONSORING MILITARY ACTIVITY
	Naval Postgraduate School Monterey, California

13. ABSTRACT

A single Fourier transform optical system was constructed and tested on two projects. First, film grain in a single Fourier transform operation was studied and a mathematical model of the film grain and a semi-quantitative prediction of the grain's transform were developed and verified using the experimental system. The film grain was found to have a noise-like spatial frequency spectrum which was a decreasing function of frequency, and that this spectrum could be considered Gaussian only in the case of fine grain films containing binary signal images. Second, the system was used to investigate a proposed method of detecting a ship wave. A deterministic relation between a ship wave and the Fourier transform of its photograph was shown to exist. A sample photograph of a ship wave was inserted into the system and operated on by a matched filter rotated in a plane normal to the optical axis. The output light intensity was determined as a function of the filter angular position. The output intensity when considered to be periodic was found to have a discernible spectral content due to the ship wave.

DD FORM 1 NOV 65 1473 (PAGE 1)

S/N 0101-807-6811

Security Classification

A-31408

14. KEY WORDS	LINK A		LINK B		LINK C	
	ROLE	WT	ROLE	WT	ROLE	WT
Character recognition						
Coherent optical system						
Data processing						
Electro-optical data processing						
Electro-optical information processing						
Film grain						
Film grain spectra						
Fourier optics						
Fourier transform						
Image processing						
Information processing						
Kelvin wave						
Noise in optical systems						
Optical data processing						
Optical filter						
Optical information processing						
Optical spatial filter						
Optical system						
Optics						
Pattern analysis						
Pattern recognition						
Photographic film						
Photographic noise						
Recognition system						
Sea surface energy spectra						
Ship detection						
Ship wave						
Ship wave detection						
Signal spectrum analysis						
Spatial filter						
Spectrum analysis						